

①
NORSAR

ROYAL NORWEGIAN COUNCIL FOR SCIENTIFIC AND INDUSTRIAL RESEARCH

Internal Report No. 1-83/84

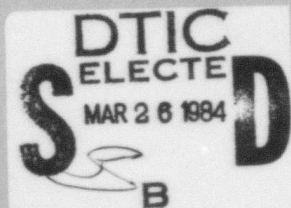
ADA139368

SEMIANNUAL TECHNICAL SUMMARY

1 April — 30 September 1983

Linda B. Tronrud (ed.)

Kjeller, December 1983



DTIC FILE COPY



DISTRIBUTION STATEMENT A

Approved for public release
Distribution Unlimited

84 03 21 103

SECURITY CLASSIFICATION OF THIS PAGE (When Data Entered)

REPORT DOCUMENTATION PAGE		READ INSTRUCTIONS BEFORE COMPLETING FORM
1. REPORT NUMBER F08606-79-C-0001	2. GOVT ACCESSION NO. AD-A139368	3. RECIPIENT'S CATALOG NUMBER
4. TITLE (and Subtitle) SEMIANNUAL TECHNICAL SUMMARY 1 April - 30 September 1983	5. TYPE OF REPORT & PERIOD COVERED 1 Apr - 30 Sep 83	
7. AUTHOR(s) L.B. Tronrud (ed.)	6. PERFORMING ORG. REPORT NUMBER Sci. Report 1-83/84	
8. PERFORMING ORGANIZATION NAME AND ADDRESS NTNF/NORSAR Post Box 51 N-2007 Kjeller, Norway	10. PROGRAM ELEMENT, PROJECT, TASK AREA & WORK UNIT NUMBERS NORSAR Phase 3	
11. CONTROLLING OFFICE NAME AND ADDRESS	12. REPORT DATE Dec 1983	
14. MONITORING AGENCY NAME & ADDRESS (if different from Controlling Office) AFTAC/HQ/TGX Patrick AFB FL 32925 USA	13. NUMBER OF PAGES 57	
16. DISTRIBUTION STATEMENT (of this Report) APPROVED FOR PUBLIC RELEASE; DISTRIBUTION UNLIMITED.	15. SECURITY CLASS. (of this report)	
17. DISTRIBUTION STATEMENT (of the abstract entered in Block 20, if different from Report)		
18. SUPPLEMENTARY NOTES		
19. KEY WORDS (Continue on reverse side if necessary and identify by block number)		
20. ABSTRACT (Continue on reverse side if necessary and identify by block number) This report describes the operation, maintenance and research activities at the Norwegian Seismic Array (NORSAR) for the period 1 April to 30 September 1983.		

The uptime of the NORSAR online detection processor system has averaged 98.8%, as compared to 95.7 for the previous period. Most of the downtime was caused by short breaks caused by resync of lines and correction of TOD-caused MODCOMP restart. A total of 2295 events were reported in this period, giving a daily average of 12.5 events. The number of reported events per month varies from 264 in April to 463 in May. There have been some difficulties with the communications lines; 03C was affected several times by power line damage, 04C was down during part of the period due to a damaged cable, and 02C was down the last part of the period due to problems on the communications line.

Improvements and modifications in the NORSAR on-line system are briefly described in Section III. Quality and uptime for the plotting system has been improved by use of a Versatec raster plotter instead of Calcomp plotters. A new disk drive has also been installed to increase the on-line data capacity from 30 to 45 hours. The ARPANET connection is again available from NORSAR.

Section IV describes field instrumentation and maintenance activities at the NORSAR Maintenance Center and includes an overview of the status of the NORESS and 02B telemetry stations.

The research activity is briefly described in Section VI. Subsection 1 presents an example of a seismic absorption band at high frequencies. Subsection 2 discusses spectral bandwidth, pulse width and moments in source analysis. Subsection 3 gives a description of experiments with temporary field installations in the new regional array during the summer of 1983 and some preliminary results from analysis of data collected. Subsection 4 discusses further developments in the Regional On-line Array Processing Package (RONAPP). Experiments involving weighted beamforming in a real time environment are presented in subsection 5.

- iii -

AFTAC Project Authorization No. : VELA VT/0702/B/PMP, Amendment 1
ARPA Order No. : 2551
Program Code No. : OF10
Name of Contractor : Royal Norwegian Council for
Scientific and Industrial Research
Effective Date of Contract : 1 October 1979
Contract Expiration Date : 30 September 1983
Project Manager : Frode Ringdal (02) 71 69 15
Title of Work : The Norwegian Seismic Array (NORSAR)
Phase 3
Amount of Contract : \$4.762.383
Contract Period Covered by the Report : 1 April - 30 September 1983

The views and conclusions contained in this document are those of the authors and should not be interpreted as necessarily representing the official policies, either expressed or implied, of the Defense Advanced Research Projects Agency, the Air Force Technical Applications Center, or the U.S. Government.

This research was supported by the Advanced Research Projects Agency of the Department of Defense and was monitored by AFTAC, Patrick AFB FL 32925, under contract no. F08606-79-C-0001.

NORSAR Contribution No. 337

DTIC
ELECTE
MAR 26 1984
S D
B

014

Accession For	
NTIS	GRA&I <input checked="" type="checkbox"/>
DTIC TAB	<input type="checkbox"/>
Unannounced	<input type="checkbox"/>
Justification	
By _____	
Distribution/ _____	
Availability Codes	
Dist	Avail and/or Special
A-1	

TABLE OF CONTENTS

	<u>Page</u>
I. SUMMARY	1
II. OPERATION OF ALL SYSTEMS --	2
II.1 Detection Processor (DP) Operation	2
II.2 Event Processor Operation	6
II.3 Array Communication	7
III. IMPROVEMENTS AND MODIFICATIONS --	11
III.1 NORSAR On-Line System using IBM 4331/4341 and MODCOMP Classic	11
IV. FIELD INSTRUMENTATION AND MAINTENANCE ACTIVITIES --	12
V. DOCUMENTATION DEVELOPED --	22
VI. SUMMARY OF TECHNICAL REPORTS/PAPERS PREPARED --	23
VI.1 Example of a seismic absorption band at high frequencies	23
VI.2 Spectral bandwidth, pulse width and moments in source analysis	29
VI.3 The new regional array: 1983 field experiments	33
VI.4 Further RONAPP developments	39
VI.5 Weighted beamforming in a real time environment	39

I. SUMMARY

This report describes the operation, maintenance and research activities at the Norwegian Seismic Array (NORSAR) for the period 1 April to 30 September 1983.

The uptime of the NORSAR online detection processor system has averaged 98.8%, as compared to 95.7 for the previous period. Most of the downtime was caused by short breaks caused by resync of lines and correction of TOD-caused MODCOMP restart. A total of 2295 events were reported in this period, giving a daily average of 12.5 events. The number of reported events per month varies from 264 in April to 463 in May. There have been some difficulties with the communications lines; 03C was affected several times by power line damage, 04C was down during part of the period due to a damaged cable, and 02C was down the last part of the period due to problems on the communications line.

Improvements and modifications in the NORSAR on-line system are briefly described in Section III. Quality and uptime for the plotting system has been improved by use of a Versatec raster plotter instead of Calcomp plotters. A new disk drive has also been installed to increase the on-line data capacity from 30 to 45 hours. The ARPANET connection is again available from NORSAR.

Section IV describes field instrumentation and maintenance activities at the NORSAR Maintenance Center and includes an overview of the status of the NORESS and 02B telemetry stations.

The research activity is briefly described in Section VI. Subsection 1 presents an example of a seismic absorption band at high frequencies. Subsection 2 discusses spectral bandwidth, pulse width and moments in source analysis. Subsection 3 gives a description of experiments with temporary field installations in the new regional array during the summer of 1983 and some preliminary results from analysis of data collected. Subsection 4 discusses further developments in the Regional On-line Array Processing Package (RONAPP). Experiments involving weighted beamforming in a real time environment are presented in subsection 5.

III. OPERATION OF ALL SYSTEMS

III.1 Detection Processor (DP) Operation

There have been 138 breaks in the otherwise continuous operation of the NORSAR online system within the current 6-month reporting interval. 60% of the stops were short breaks that lasted for no more than two minutes. These breaks were not caused by the complete DP system going down, rather by resync of lines and correction of TOD-caused MODCOMP restart. The uptime percentage for the period is 98.8 per cent as compared to 95.7 for the previous period.

Fig. III.1.1 and the accompanying Table III.1.1 both show the daily DP downtime for the days between 1 April and 30 September 1983. The monthly recording times and percentages are given in Table III.1.2.

The breaks can be grouped as follows:

a)	Stops related to program work and errors	77
b)	Hardware maintenance	2
c)	Power breaks	5
d)	TOD correction	33
e)	Array monitoring	6
f)	MODCOMP failure	14
g)	Disk failure	1

The total downtime for the period was 54 hours and 36 minutes. The mean-time-between-failures (MTBF) was 1.3 days as compared with 2.9 days for the previous period.

J. Torstveit

DAY	START	STOP	COMMENTS.....	DAY	START	STOP	COMMENTS.....
99	19	45	19 MCDCCMP FAILURE	129	11	52	11 DP SOFTWARE
99	21	33	21 MCDCCMP FAILURE	136	11	24	21 MCDCCMP FAILURE
100	12	49	12 MCDCCMP FAILURE	144	7	23	7 DP SOFTWARE
100	11	59	11 MCDCCMP FAILURE	144	8	41	9 POWER BREAK
100	12	32	13 MCDCCMP FAILURE	147	12	52	15 DP SOFTWARE
100	14	14	14 MCDCCMP FAILURE	152	13	1	13 2 TOD CORRECTION
100	15	58	16 MCDCCMP FAILURE	160	15	33	15 34 LCD CORRECTION
100	17	61	18 MCDCCMP FAILURE	162	12	42	12 44 LCD CORRECTION
100	19	24	24 MCDCCMP FAILURE	164	6	22	6 23 100 CORRECTION
100	21	8	24 MCDCCMP FAILURE	165	6	2	6 3 LCD CORRECTION
100	22	22	23 MCDCCMP FAILURE	166	6	9	6 10 LCD CORRECTION
101	1	35	6 MCDCCMP FAILURE	166	12	49	24 5 DISK FAILURE
103	6	47	12 MAINTENANCE	167	12	36	6 26 DISK FAILURE
104	13	6	13 MAINTENANCE	167	12	36	12 46 DP SOFTWARE
104	21	29	21 MCDCCMP FAILURE	174	11	6	11 7 LCD CORRECTION
106	7	21	7 DP SOFTWARE	187	6	2	6 3 LCD CORRECTION
108	3	14	9 DP SOFTWARE	187	12	33	12 34 100 CORRECTION
108	10	17	15 DP SOFTWARE	182	6	57	6 59 LCD CORRECTION
108	11	15	13 DP SOFTWARE	185	11	59	12 3 SYSTEM WORK
116	8	9	8 POWER BREAK	186	13	48	13 5 SYSTEM WORK
119	13	40	14 DP SOFTWARE	189	5	53	5 54 100 CORRECTION
119	20	7	20 9 DP SOFTWARE	189	6	2	6 3 LCD CORRECTION
119	21	39	21 41 DP SOFTWARE	189	12	47	12 48 SYSTEM WORK
119	23	8	23 35 DP SOFTWARE	193	23	42	23 43 SYSTEM WORK (IPL 4341)
119	23	33	23 35 DP SOFTWARE	196	6	13	6 14 TOD CORRECTION
120	0	42	0 44 DP SOFTWARE	196	7	19	7 20 LCD CORRECTION
120	1	4	1 6 DP SOFTWARE	196	7	53	7 54 LCD CORRECTION
120	2	14	2 16 DP SOFTWARE	198	8	49	8 50 LCD CORRECTION
120	2	37	2 39 DP SOFTWARE	200	9	4	9 5 TOD CORRECTION
120	4	7	4 10 DP SOFTWARE	202	12	43	12 44 SYSTEM WORK
120	5	35	5 38 DP SOFTWARE	203	7	14	7 15 LCD CORRECTION
120	7	11	7 13 DP SOFTWARE	213	9	40	9 41 SYSTEM WORK
122	5	27	6 21 POWER BREAK	214	11	31	11 32 TOD CORRECTION
123	5	27	6 42 POWER BREAK	217	17	9	19 17 POWER BREAK
129	8	8	8 10 DP SOFTWARE	220	13	37	13 38 LCD CORRECTION
129	11	23	11 25 DP SOFTWARE	221	6	1	6 2 LCD CORRECTION

Table 11.1 List of breaks in NP processing in the period 1 April - 30 September 1983.

DAY	START	STOP	COMMENTS.....	STCP	COMMENTS.....
223	6	2	6 3 TCD CORRECTION	241	13 48 11 49 TCD CORRECTION
223	8	8	9 SYSTEM WCRK	242	11 41 11 42 SYSTEM WORK
223	13	8	16 SYSTEM WCRK	243	13 4 11 43 SYSTEM WCRK
223	8	21	27 SYSTEM WCRK	243	11 4 11 1 SYSTEM WCRK
223	9	51	6 33 SYSTEM WCRK	243	11 4 11 6 SYSTEM WCRK
223	8	44	8 45 SYSTEM WCRK	244	0 32 6 34 TCD CORRECTION
223	9	55	8 58 SYSTEM WCRK	244	1 33 1 34 TCD CORRECTION
223	9	6	9 7 SYSTEM WCRK	248	8 47 8 49 TCD CORRECTION
223	9	21	9 32 SYSTEM WCRK	248	3 51 1 6 SYSTEM WCRK
223	9	48	9 51 SYSTEM WCRK	248	13 8 11 9 SYSTEM WORK
223	5	52	9 52 SYSTEM WCRK	248	13 1 11 11 SYSTEM WCRK
223	13	5	13 34 SYSTEM WCRK	248	13 14 13 23 SYSTEM WCRK
223	12	58	12 59 DP PROG	249	14 31 14 33 SYSTEM WCRK
224	13	7	13 8 SYSTEM WCRK	249	14 41 14 47 SYSTEM WCRK
224	12	37	12 39 TCD CORRECTION	252	12 48 12 49 TCD CORRECTION
225	6	29	6 30 TCD CORRECTION	256	8 49 8 57 SYSTEM WORK
229	7	37	7 38 SYSTEM WCRK	258	7 41 7 45 ARRAY MONITORING
229	7	42	7 54 SYSTEM WCRK	258	7 49 7 54 ARRAY MONITORING
229	7	57	8 2 SYSTEM WCRK	258	13 12 13 13 ARRAY MONITORING
229	12	16	12 17 DP PROG	258	13 14 13 18 ARRAY MONITORING
230	14	23	14 32 SYSTEM WCRK	258	14 48 14 49 ARRAY MONITORING
231	9	17	9 24 SYSTEM WCRK	262	6 13 6 12 ARRAY MONITORING
231	5	34	9 34 SYSTEM WCRK	262	9 18 9 22 SYSTEM WCRK
231	10	23	13 26 SYSTEM WCRK	262	9 48 9 51 SYSTEM WCRK
231	12	43	12 46 DP PROG	263	11 51 11 52 TCD CORRECTION
234	9	6	9 7 SYSTEM WCRK	266	15 49 15 53 TCD CORRECTION
234	9	15	9 17 SYSTEM WCRK	269	6 52 6 53 TCD CORRECTION
234	10	20	10 23 SYSTEM WCRK	270	6 58 6 59 SYSTEM WCRK
234	10	27	10 29 SYSTEM WCRK	270	7 27 7 28 SYSTEM WCRK
234	10	39	10 43 SYSTEM WCRK	271	12 44 12 45 SYSTEM WORK
234	11	21	11 25 SYSTEM WCRK	271	6 47 6 48 TCD CORRECTION
234	11	56	12 1 SYSTEM WCRK		
234	12	8	12 16 SYSTEM WCRK		
234	12	18	12 21 SYSTEM WORK		
234	12	35	12 36 SYSTEM WCRK		
261	6	10	6 11 TCD CORRECTION		

*** NUMBER OF BREAKS = 138
 *** MEAN TIME BETW. FAILURES = 1.3 DAYS
 *** NUMBER OF UPTIME INTERVALS = 139

Table II.1.1 (cont.)

- 5 -

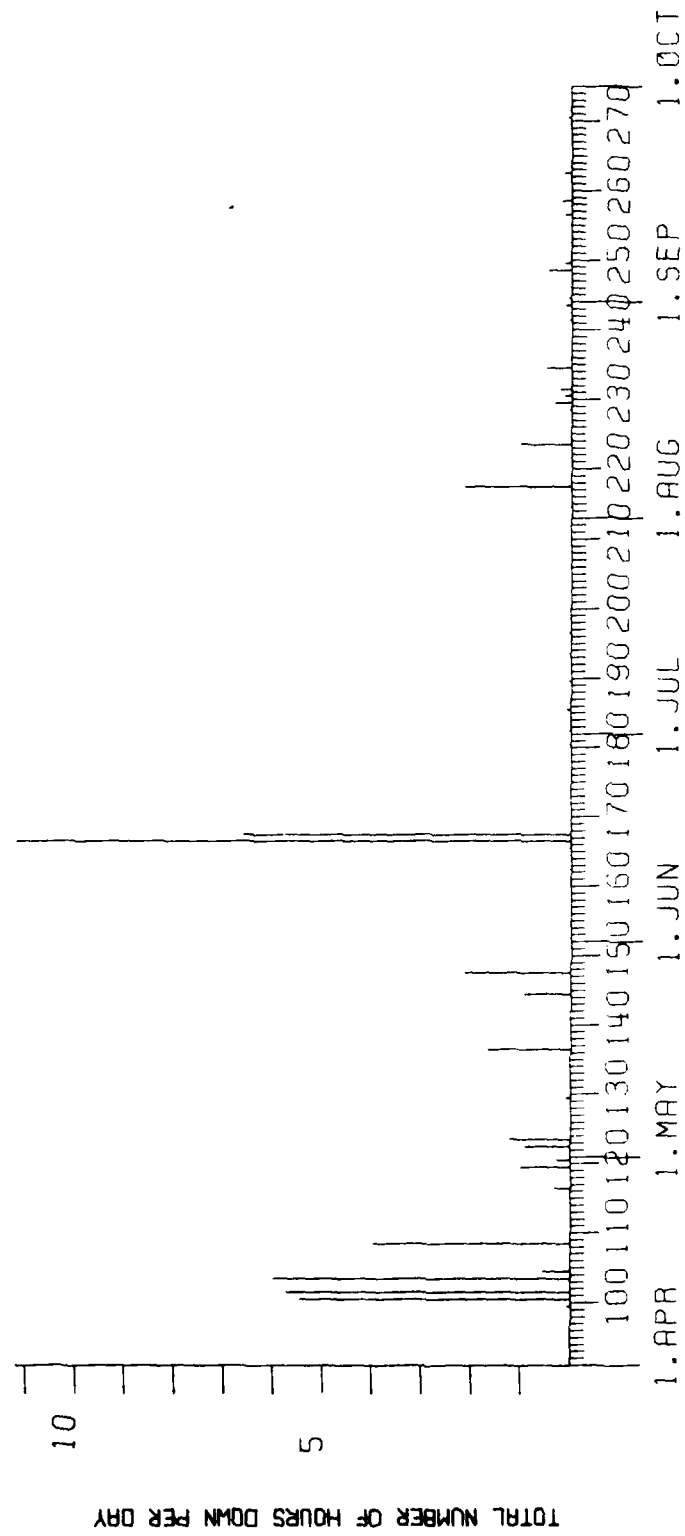


Fig. II.1.1 Detection Processor downtime in the period 1 April - 30 September 1983.

Month	DP Uptime (hrs)	DP Uptime (%)	No. of DP Breaks	No. of Days with Breaks	DP MTBF* (days)
Apr	697.15	96.8	32	9	0.9
May	737.00	99.1	9	6	3.1
Jun	702.03	97.5	11	9	2.4
Jul	743.42	99.9	14	10	2.1
Aug	739.25	99.4	46	15	0.7
Sep	718.46	99.8	26	12	1.1
	4338.11	98.8	138	61	1.3

*Mean-time-between-failures = (Total uptime/No. of up intervals)

TABLE II.1.2

Online System Performance
1 April - 30 September 1983

II.2 Event Processor Operation

In Table II.2.1 some monthly statistics of the Event Processor operation are given:

	Teleseismic	Core Phases	Sum	Daily
Apr 83	264	60	324	10.8
May 83	463	56	519	16.7
Jun 83	317	67	384	12.8
Jul 83	313	82	395	12.7
Aug 83	320	56	376	12.1
Sep 83	265	32	297	9.9
	1942	353	2295	12.5

TABLE II.2.1

B. Kr. Hokland

II.3 Array Communication

Table II.3.1 reflects the performance of the communications system throughout the reporting period.

High figures as indicated in the table are related to incidents such as power line damage (03C), NORESS usage of the original 06C line, and damaged cable (04C). Otherwise communication systems have been most reliable.

Summary

April: Apart from an incident in connection with 06C communication system (week 16), reliable performance.

May: NORESS data transferred via the 06C original communication path; otherwise reliable performance.

June: Unwanted noise observed on the 04C communication line (27 June). Test carried out (29 June) did not reveal irregularities, but situation changed (30 June). Transmitted commands had no influence on the CTV modem. NTA/Lillestrøm notified. 06C communication path still in NORESS usage.

July: 04C back in operation after NTA/Hamar had replaced part of the communication cable between the CTV and the local central.

August: A line problem caused 02C outage between 12-15 August. 03C dropped out (29 August), and remained so for the rest of the period. Remaining system reliable performance.

September: 03C back in operation 15 September after a power outage. The same subarray lost its power again (26 September, also this time caused by falling trees over the power line). 02B was out of operation 27-28 September due to NTA/Lillestrøm work.

Table II.3.2 indicates distribution of outages with respect to the individual subarrays.

Miscellaneous

The new line to be used in connection with the NORESS array was not operational until mid-July, although NTA/Hamar and Lillestrøm were engaged in May and June. Main reason for the delay was unexpected attenuations in parts of the line between Hamar and the array.

As far as the temporary NORESS array and 02B (telemetry) installation is concerned, we have observed a few minor problems, such as: spikes and reduced performance on NORESS channels 02, 03, 12 and 13 (week 19)

Reduced performance on ch. 12 (NORESS) (week 39).

NORESS channels 17-22 out of operation for 2 days (week 39). Heavy attenuation on ch. 27, 02B (telemetry), Sept 1 (week 39).

O.A. Hansen

Sub- Array	APR (4) (4.4-1.5)	MAY (5) (1.5-5.6)	JUN (4) (6.6-3.7)	JUL (4) (4-31.7)	AUG (5) (1.8-4.9)	SEP (4) (4.9-2.10)	AVERAGE YEAR
01A	0.005	0.021	0.028	0.001	0.005	0.005	0.011
01B	0.004	0.023	0.027	0.002	0.005	0.005	0.011
02B	0.005	0.023	0.027	0.002	0.004	3.58	0.61
02C	0.005	-	0.093	0.002	0.71	0.004	0.14
03C	0.005	0.055	0.128	*3.52	*20.0	*52.7	*12.73
04C	0.005	0.022	*7.714	*33.08	0.14	0.01	*6.87
06C	0.23	*2.07	*100.0	*81.09	*100.0	*100.0	*63.89
AVER	0.04	0.3	15.4	16.8	17.3	22.3	12.0
				04C	03C	03C	03C
LESS			06C	06C	06C	06C	06C
	-	-	1.3	0.7	0.2	0.7	1.5

* See item II.3 (array communications) regarding figures with asterisks.

TABLE II.4.1

Communications performance. Figures in per cent, based on
total transmitted frames/week (1.2096×10^7).
(4 Apr - 30 Sep 83)

Week/ Year	Subarray/percent outage						
	01A	01B	02B	02C	03C	04C	06C
14/83	0.020	0.020	0.020	0.020	0.020	0.020	0.020
15	-	-	-	-	-	-	-
16	-	-	-	-	-	-	4.3
17	0.020	0.001	0.002	-	0.002	0.001	0.9
18	-	-	-	-	-	-	6.4
19	-	-	-	-	-	-	3.55
20	0.070	0.060	0.090	-	0.015	0.060	0.4
21	0.035	0.020	0.025	-	0.120	0.050	0.04
22	-	-	-	-	0.04	0.03	100.0
23	0.08	0.11	0.074	0.370	0.085	0.08	100.0
24	0.03	0.002	0.04	-	0.04	0.03	100.0
25	-	-	-	-	0.38	0.13	100.0
26	-	-	-	-	0.01	30.6	100.0
27	0.002	0.0023	0.0024	0.0015	0.002	71.4	100.0
28	-	-	-	-	0.08	60.8	76.1
29	0.0001	0.0013	0.001	0.0013	0.0013	0.005	48.3
30	0.002	0.003	0.003	0.0034	0.004	0.10	100.0
31	0.0002	-	-	0.0004	-	0.014	100.0
32	-	-	-	-	-	0.2	100.0
33	0.001	0.0015	0.001	3.6	0.001	1.8	100.0
34	0.001	0.001	0.001	0.0014	0.003	0.03	100.0

TABLE II.4.2
Subarray/percent outage

III. IMPROVEMENTS AND MODIFICATIONS

III.1 NORSAR on-line system using IBM 4331/4341 and MODCOMP Classic

We refer to the detection processor operation statistics for detailed performance of the new system.

During this reporting period there have been unit checks between MODCOMP and the 4331 computer. The follow-up result of this is periodic loss of a 0.5 sec data block. At the moment we cannot say where the problem is located. However, we expect a solution of the communication problem when we interface the MODCOMP directly to the 4331 channel. At the moment we have connected the MODCOMP computer directly to the channel and the operating system on IBM has accepted the device which simulates a tape drive. We have also done some read/write tests.

The quality and uptime for the plotting system has been improved. We are now using a 10" Versatec raster plotter instead of the Calcomp plotters. The Versatec is connected through the Series/1 front-end processor. The 4341 system does the vector-to-raster converting and transmit raster lines to the Series/1 processor which does the plotting on the Versatec.

The ARPANET connection is again available from NORSAR. At the moment we have a direct line to a VAX-computer, which is connected to the ARPANET as a host machine. The user-id for NORSAR is FRODE and the machine id is NTA-VAX. The next step in this ARPANET connection is a host connection at NORSAR. We will probably use an IBM personal computer for this. When we have the host connection, it will be possible to transfer data files directly from the main system through the ARPANET.

We have also installed a new disk drive to keep more data on-line. At the moment we have a capacity of 30 hours with on-line data. With the new disk drive we may store 45 hours with on-line data.

R. Paulsen

IV. FIELD INSTRUMENTATION AND MAINTENANCE ACTIVITIES

Improvements and modifications

Reference is made to Table IV.1 and IV.2 indicating the status of the SP instruments (original array), the modified NORESS array, and the expanded 02B subarray (telemetry stations).

Since the last report the NORESS array has been subject to a number of changes.

5 June: Five sites (see Table VI.2) were equipped with 3-component SP seismometers S-13, as a temporary experiment to collect SP data recorded at NORSAR. The array was operational 10 June, and the operation was terminated 5 July. Otherwise refer to Fig. IV.1 and Table IV.3, which indicate station numbering and geographical coordinates, respectively.

23 July: The new temporary NORESS array was fully operational, equipped with vertical seismometers S-13 at 12.5 Hz, occupying NORSAR analog channels 1-21, wind speed data on ch. 22 (see Table IV.2). Reference is also made to Fig. IV.2, and Table IV.4, which indicate station numbering and geographical coordinates, respectively.

02B (telemetry) st. 1-6 equipped with seismometers S-500, now occupy ch. 23-28 (see Table IV.2 and in addition Fig. IV.3 and Table IV.5).

Planning with regard to the permanent NORESS is going on. Meetings have been held between representatives from Sandia, a consultant company and NORSAR.

Activities in the field and at the Maintenance Center

This section outlines in brief the activities in the field and at the NORSAR Maintenance Center. Table IV.6 indicates other activities in the field and at the NMC.

Corrective/preventive maintenance in the original array has been limited to replacement of 33 RA-5 amplifiers in the well head vaults, and replacement of a remote centering device (mass position) on an LP instrument.

Array status

As of 30 September 1983 the following channels deviated from tolerances:
01B05; 02B05; 02C06; 03C01,08; 06C all channels (not used).

- 01A 01 8 Hz filter
- 02 -"- , 60 m hole
- 03 Wind speed measurements
- 04 Attenuated 40 dB
- 05 Wind direction measurements.

O.A. Hansen

Subarray (Normally)	Instr. no. within SA	Ch. no. on NORSAR data tape	Status / Time of changes
01A (1)	1	1	8 Hz filter (10/29/82) 1) (10/08/82) 2) (10/28/82) 3) (10/28/82) Normal
	2	2	
	3	3	
	4	4	
	5	5	
	6	6	
01B (2)	1	7	
	2	8	
	3	9	
	4	10	
	5	11	
	6	12	
02B (3)	1	13	
	2	14	
	3	15	
	4	16	
	5	17	
	6	18	
02C (4)	1	19	
	2	20	
	3	21	
	4	22	
	5	23	
	6	24	
03C (5)	1	25	
	2	26	
	3	27	
	4	28	
	5	29	
	6	30	

Note: 1) Data from borehole at site 1 (60 m hole) to SP ch 02 (in CTV).
2) Wind speed to SP ch 03 (in CTV).
3) Wind direction to SP ch 05 (in CTV).

TABLE IV.1
Status of NORSAR SP instruments recorded on data tape.

Subarray (Normally)	Instr. no. within SA	Ch. no. on NORSAR data tape	Status / Time of changes
04C (6)	1	31	
	2	32	
	3	33	
	4	34	
	5	35	
	6	36	
06C (7)	1	37 4)	
	2	38	
	3	39	
	4	40	
	5	41	
	6	42	

Note: 4) 06C com. line used for transfer of NORESS data to NDPC.

TABLE IV.1 (cont.)

Subarray	NORSAR	Time of Change	
		06/10/83	07/23/83
06C	1	NORESS st. no. 2, VERT S-13	NORESS st. no. AO, VERT seis S-13 +
NORESS	2	" 2, NS S-13	" A1
(temporary)	3	" 2, EW S-13	" A2
	4	" 1, VERT S-13	" A3
	5	" 1, NS S-13	" B1
	6	" 1, EW S-13	" B2
	7	" 6, VERT S-13	" B3
	8	" 6, NS S-13	" B4
	9	"	" B5
	10	"	" C1
	11	"	" C2
	12	"	" C3
	13	"	" C4
	14	"	" C5
	15	NORESS st. no. 6, EW S-13	" C6
	16	" 9, VERT S-13	" C7

* Operational 10 June - 5 July 83
+ 12 Hz

1) Omitted 5 June 1983
2) Changed 5 June 1983

TABLE IV.2

Status of NORESS and O2B (telemetry stations) and their connections to analog channels
at NDPC (1-28)

Subarray Normally at NDPC	NORSAR Analog ch.	Time of Change	
		06/10/83	07/23/83
*	*		
06C	17	NORESS st. no. 9, NS S-13	NORESS st. no. D1, VERT seis S-13+
NORESS	18	" " 9, EW S-13	D2 " "
(temporary)	19	" " 11, VERT S-13	D4 " "
	20	" " 11, NS S-13	D5 " "
	21	" " 11, EW S-13	D7 " "
	22		Wind speed at A0
	23		02B (telem.) 1 S-500
	24		" " 2 "
	25		" " 3 "
	26		" " 4 "
	27		" " 5 "
	28		" " 6 "
* Operational 10 June - 5 July 83			
+ 12 Hz			

TABLE IV.2 (cont.)

St. no.	NS (m)	EW (m)
2	0	0
1	271	-62
6	-348	-219
9	-407	-660
11	1232	-502

TABLE IV.3
Temporary 5-site 3-component SP seismometer
experimental array.

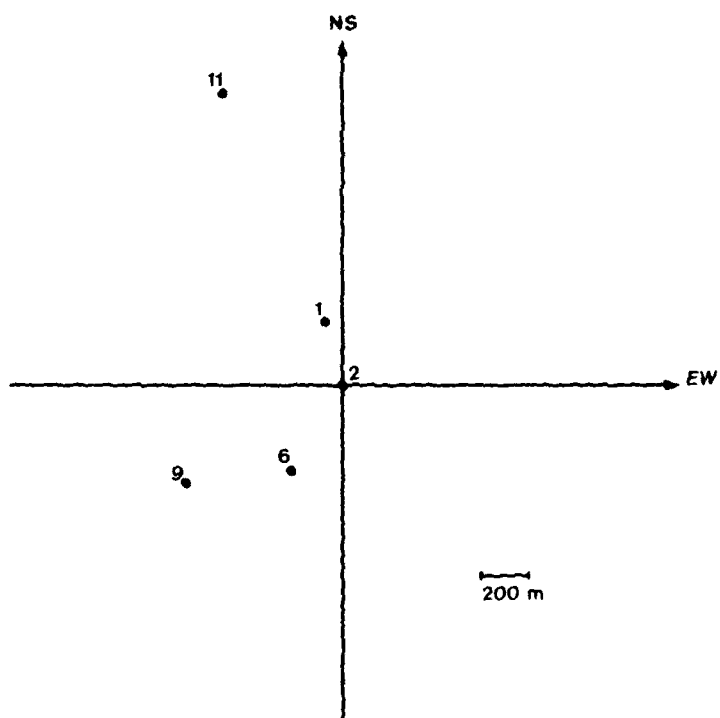


Fig. IV.1

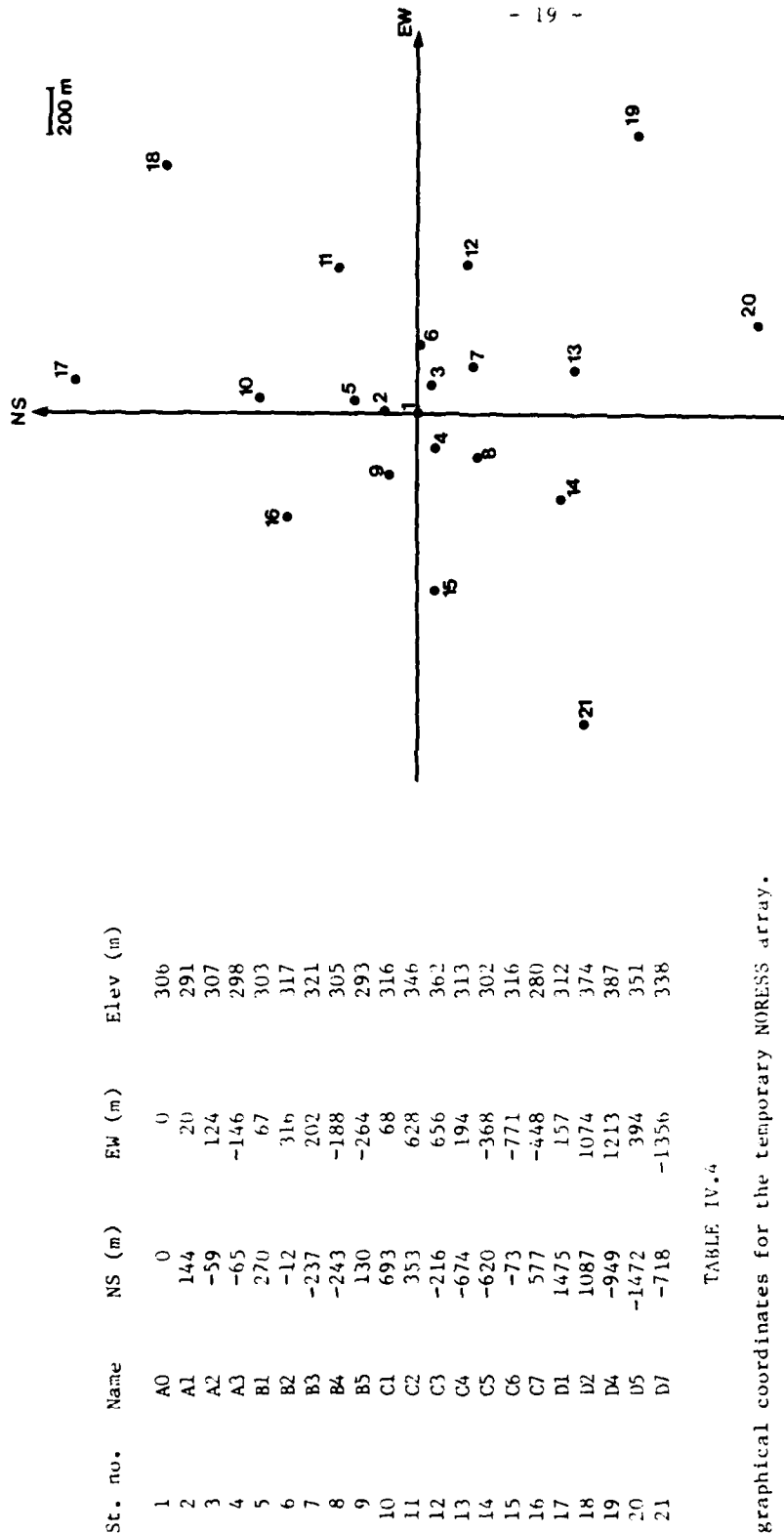


TABLE IV.

Geographical coordinates for the temporary NORESS array.

Fig. IV.2 Station numbering in the temporary NORESS array.

Station No.	Latitude (N.)	Longitude (E.)
1	61.068344	11.156468
2	61.101196	11.161124
3	61.091309	11.166824
4	61.107315	11.174083
5	61.084824	11.174442
6	61.049728	11.158080

TABLE IV.5

Preliminary geographical coordinates
for the new 02B stations.

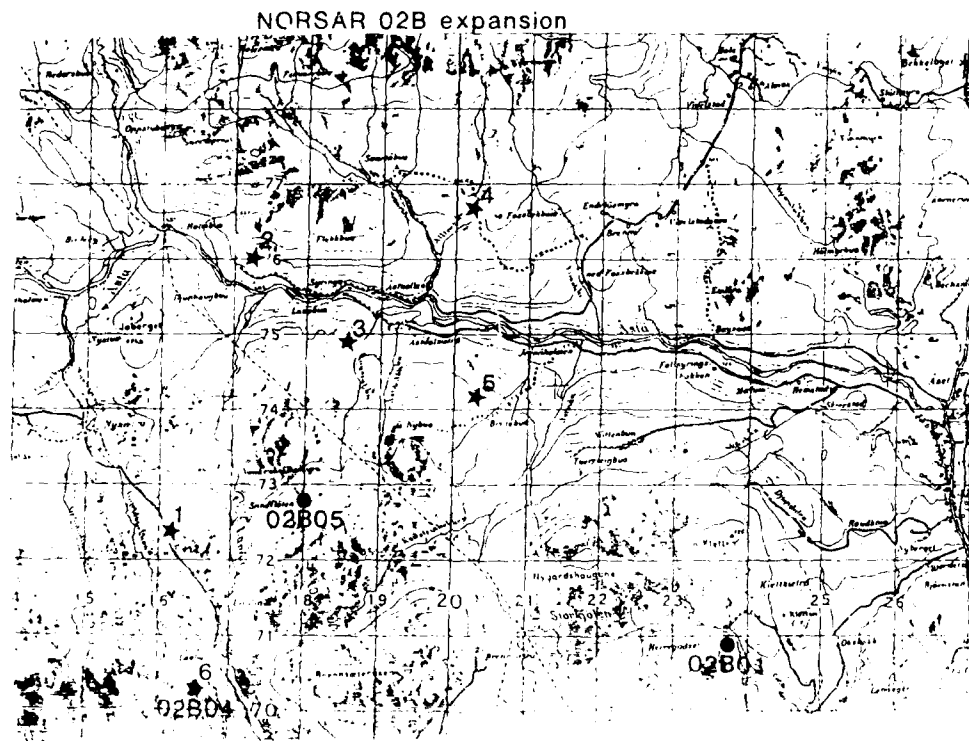


Fig. IV.3 The six new stations in the expanded O2B array.

SA/Area	Task	Date
06C NORESS	Activities related to expansion of the NORESS array	(Apr.) (Weeks 18,19 May)
06C NORESS	Installation of 3-component SP-seism. SS-1 on five new stations	(" 20,21 May)
06C NORESS	Activities rel. to expansion of NORESS array continued involving attempt to find a possible location for the RT and calculating different fiber optic cable lengths	(June)
04C area	Replaced part of com. cable	(1 Jul)
01A	Battery bank electrolyte replaced	(27 Jul)
01B	"	(")
01A	Noise data recording (ch. 1 and 60 m hole)	(start 28 Jul)
02B	Battery band electrolyte replaced	(29 Jul)
04C	Cable splicing SP00. Protection card replaced.	(2 Aug)
06C	Battery bank electrolyte replaced	(3 Aug)
01B	Cable splicing SP03 area	(4 Aug)
04C	Cable mending near SP01	(8,9 Aug)
01A	RA-5 replacement	(11 Aug)
02B	"	(12 Aug)
04C	RA-5 replacement (03). Battery bank electrolyte replaced	(15 Aug)
03C	Battery bank electrolyte replaced	(16 Aug)
04C	Remaining RA-5 ampl. replaced	(17 Aug)
02C	Battery bank electrolyte replaced	(18 Aug)
04C	Remote Centering Device (RCD) Vert. LP seism. replaced	(22 Aug)
06C	Jobs of different character carried out	(25,26 Aug)
06C	Different tasks related to profile blasting	(29 Aug)
02C	RA-5 replacement except 01,02	(30 Aug)
06C	Profile blasting in the NORESS array (5 men) in connection with a seismic reflection survey	(30 Aug)
NMC	Property control by J. Guy Turner Det 16 AFCMC, Wiesbaden	(12 Sept)
03C	SA visit in connec. with power failure	(14 Sept)
01B	RA-5 ampl. replaced all SP points	(20 Sept)
03C	" (-SP04)	(21 Sept)
03C	Faulty cal. amp. cir. repaired (SP01)	(23 Sept)
06C	Reported line fault checked	(29 Sept)
03C	SA visited in connection with loss of data; found power line broken	(29 Sept)

TABLE IV.6

Activities in the field and at NORSAR Maintenance Center.
(1 April - 30 September 1983)

V. DOCUMENTATION DEVELOPED

Doornbos, D.J.: On the determination of radiated energy and related source parameters, submitted for publication.

Husebye, E.S. and E. Thoresen: Personal seismometry now, submitted for publication.

Tronrud, L.B., 1983: Semiannual Technical Summary, NORSAR Sci. Rep. No. 2-82/83, NTNF/NORSAR, Kjeller, Norway.

Tryggvason, K. and E.S. Husebye: Seismic image of the hypothesized Icelandic hot spot, Tectonophysics, in press.

L.B. Tronrud

VI. SUMMARY OF TECHNICAL REPORTS/PAPERS PREPARED

VI.1 Example of a seismic absorption band at high frequencies

There is growing evidence that, in most regions of the earth, seismic absorption in terms of $Q^{-1}(\omega)$ forms a band centered at relatively low frequencies, i.e., the high-frequency cut-off of this absorption band is in the range of short-period body waves (0.2-1.0 Hz) (Doornbos, 1983). One should nevertheless consider the possibility that the absorption band is at higher frequencies in those regions which are known to be highly absorptive, or 'low-Q' (e.g., Anderson and Given, 1982). Examples of such regions are thought to be the upper mantle low-velocity zone, the region near the base of the mantle (the D" layer) and the region near the top of the inner core. Observational verification is usually difficult, but the relative amplitudes and waveforms of some short-period core phases provide an interesting case. Short-period NORSAR records show a characteristic change of the PKIKP waveform passing through the inner core, as compared to PKP_{BC} bottoming above. One can attribute this change to the effect of absorption in the inner core, provided adequate care is taken to avoid frequency-dependent elastic effects, to avoid source effects and to eliminate receiver structure effects. We have used full NORSAR array beams to eliminate near-receiver effects, and this limits our analysis to events between 1971-1976, when the array still had its full size. Fig. VI.1.1 shows PKIKP and PKP_{BC} from three such events in the distance range 147-151°. The two phases are characteristically different, but they should have a similar waveform apart from absorption effects. By verifying that the Hilbert transform of PKP_{BC} is similar to the PKP_{AB} waveform, it can be concluded that the anomalous waveshape is in PKIKP. To investigate this effect we convolved PKP_{BC} with an absorption band operator characterizing transmission through the inner core; we also corrected the amplitude ratio due to purely elastic effects. The required inner core absorption band turns out to be on the high-frequency side of the data. Absorption bands encompassing the data (a 'constant Q' model) or on the low-frequency side of it (the more usual absorption band) are unsuccessful. Fig. VI.1.2.a-c illustrate the effect of typical examples of such absorption bands. The conclusion

is that for absorption in the inner core, the low-frequency cut-off of the band $(2\pi\tau_2)^{-1}$ is above 2 Hz, and minimum Q_α in the center of the band is likely to be below 100. The intrinsic dissipation can be in shear and/or in bulk. Recently proposed bulk dissipation mechanisms where the governing equations are diffusive (Loper and Fearn, 1983) have consequences for the high-frequency side of the absorption band. However, with the relative position of the inner core absorption band as inferred here, the differences are unlikely to be observable.

D.J. Doornbos

References

Anderson, D.L. and J.W. Given, 1982: Absorption band Q model for the earth, *J. Geophys. Res.* 87, 3893-3904.

Doornbos, D.J., 1983: Observable effects of the seismic absorption band in the earth, *Geophys. J. R. Astr. Soc.*, in press.

Loper, D.E. and D.R. Fearn, 1983: A seismic model of a partially molten inner core, *J. Geophys. Res.*

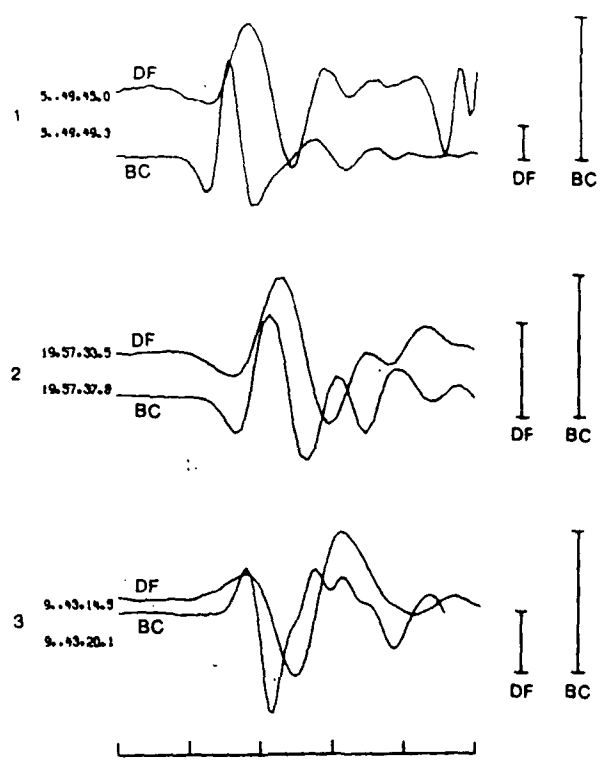


Fig. VI.1.1 NORSAR array beams with PKIKP(DF) and PKP(BC) from three events in the distance range 147-151°. Relative times adjusted to the first peak or trough. Record length is 5 seconds. The relative amplitude scaling is indicated to the right.

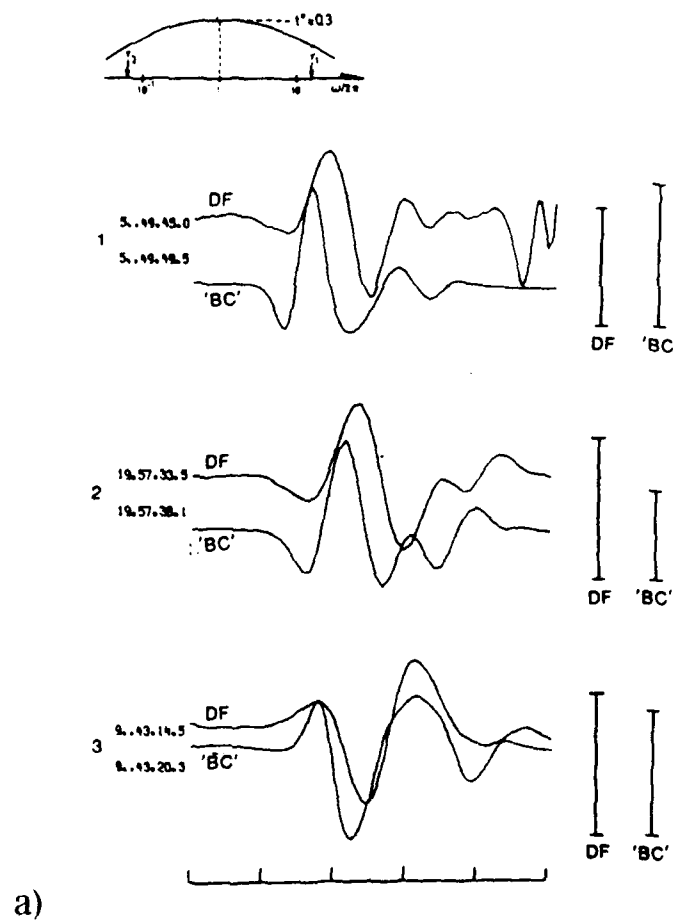


Fig. VI.1.2 Observed PKIKP(DF) compared with synthetic derived from PKP(BC) by correcting for relative path effects, including absorption in the inner core. Other details as in Fig. VI.1.1. Inner core absorption bands are specified by: (a) $t_m^* = 0.3$ s, $(2\pi\tau_1)^{-1} = 0.0625$ Hz, $(2\pi\tau_2)^{-1} = 16$ Hz; (b) $t_m^* = 1.0$ s, $(2\pi\tau_2)^{-1} = 0.002$ Hz, $(2\pi\tau_1)^{-1} = 0.5$ Hz; (c) $t_m^* = 1.4$ s, $(2\pi\tau_2)^{-1} = 4$ Hz, $(2\pi\tau_1)^{-1} = 40$ Hz.

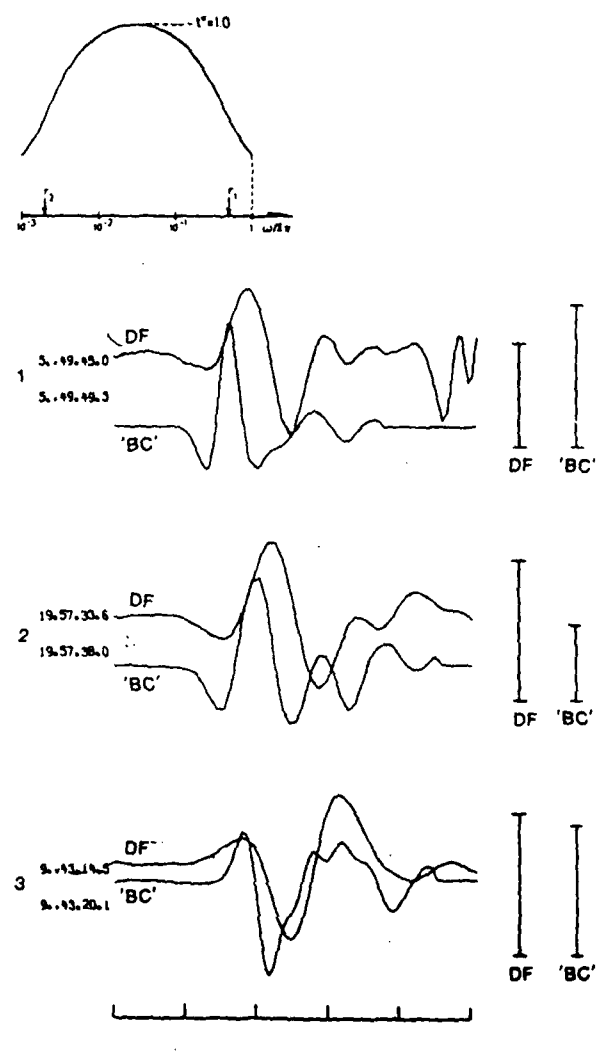
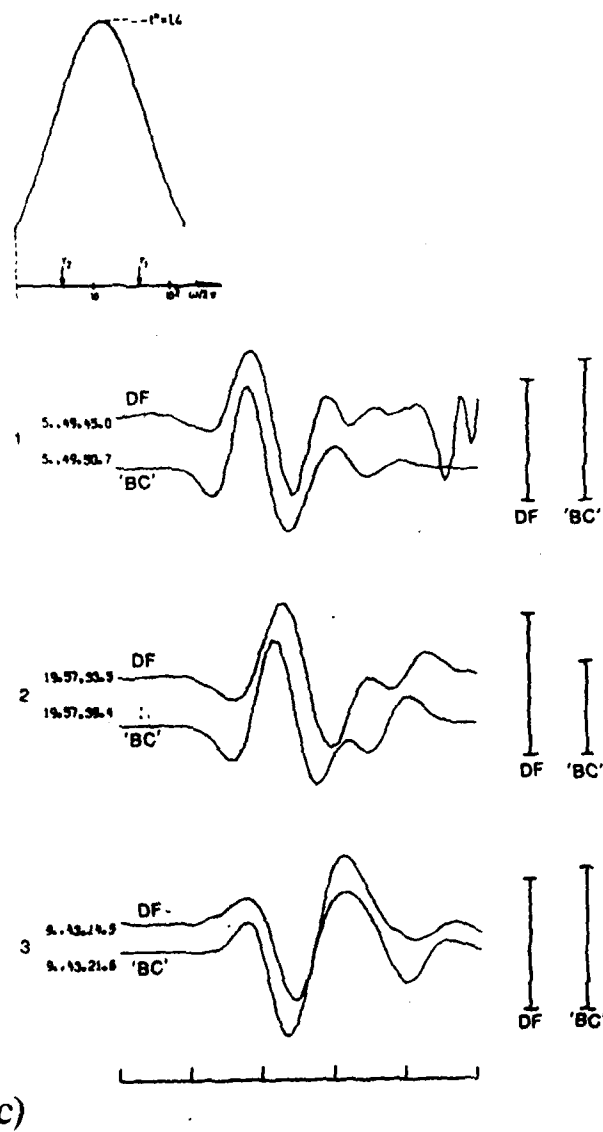


Fig. VI.1.2



c)

Fig. VI.1.2

VI.2 Spectral bandwidth, pulse width and moments in source analysis

An observational parameter often employed in source analysis is the spectral bandwidth (usually inferred from a corner frequency in the spectrum); for example radiated energy is proportional to a weighted average of the spectral bandwidth squared. On the other hand, a measure of source size is given by the time domain pulse width (more precisely, the second central moment of the pulse). Although these two parameters are simply related for any point on the focal sphere, the effect of averaging can be quite different.

It is possible to discuss this effect in the context of a moment tensor representation of the source. If the temporal derivative of stress glut is approximated (Doornbos, 1982):

$$\dot{m}_{jk}(\xi, \tau) = M_{jk} f(\xi, \tau) \quad (1)$$

then the scalar function $f(\xi, \tau)$ can be expanded in moments. If we choose as the reference point the 'center of gravity' or 'centroid' (ξ_0, τ_0) of $f(\xi, \tau)$, then the expansion is in terms of the central moments. We cancel the observationally troublesome phase effect by relating the moments to the amplitude density spectrum of a (normalized) pulse $f(\tau)$:

$$|F(\omega)|^2 = 1 - \omega^2 F_{(2)} + \frac{1}{12} \omega^4 (\hat{F}_{(4)} + 3 \hat{F}_{(2)}^2) + \dots \quad (2)$$

and directivity is included in the model by replacing

$$f(\tau) \text{ by } f(\tau, \xi), \hat{F}_{(2)} \text{ by } \xi^T \hat{F}_{(2)} \xi, \text{ etc.}$$

Here ξ is a generalized slowness vector as defined in Doornbos (1982). For practical purposes it is necessary to reduce the number of parameters, and this is done by means of a suitable extrapolation of the spectrum based on the second central moments. The Gaussian and ω -square models are representative examples.

The corner frequency has been conventionally determined as an average over the focal sphere. Similarly we can form the averaged spectral bandwidth for P and S waves:

$$\bar{B}_c = \frac{1}{4\pi} \int_{\Omega} B(\xi_c) d\Omega \quad (3)$$

where c is the P or S velocity. The result will depend on the directivity of $f(\xi, \tau)$, in particular on the effect of rupture velocity. In contrast, the averaged pulse width squared is related to

$$\bar{F}_c = \frac{1}{4\pi} \int_{\Omega} \xi_c^T \hat{F}(2) \xi_c d\Omega = \frac{1}{3c^2} (\hat{F}_{xx} + \hat{F}_{yy} + \hat{F}_{zz}) + \hat{F}_{tt} \quad (4)$$

where \hat{F}_{ii} are the diagonal components of $\hat{F}(2)$. This result does not explicitly involve rupture velocity. As a measure of pulse width we will use $\bar{D}_c = \chi \bar{F}_c^{\frac{1}{2}}$, with χ a (model dependent) constant. Usually an inverse square root relation between B and $\hat{F}(2)$ exists for any point on the focal sphere, but for sources with strong directivity effects (e.g., Haskell type of models), the result of averaging procedures (3) and (4) can be quite different. This is illustrated by comparing Figs. VI.2.1 and VI.2.2, which give results for moment tensor approximations to a Haskell bidirectional model with aspect ratio 0.4 and to a circular model, respectively. The 'corner frequency shift' in terms of \bar{B}_a/\bar{B}_b is also illustrated in these figures (c.f. Hanks, 1981). \bar{F}_c can be related to source finiteness, and \bar{B}_c to the dominant frequency range for energy radiation.

D.J. Doornbos

References

Doornbos, D.J., 1982: Seismic source spectra and moment tensors, *Phys. Earth Planet. Inter.* 30, 214-227.

Hanks, T.C., 1981: The corner frequency shift, earthquake source models, and Q, *Bull. Seism. Soc. Am.* 71, 597-612.

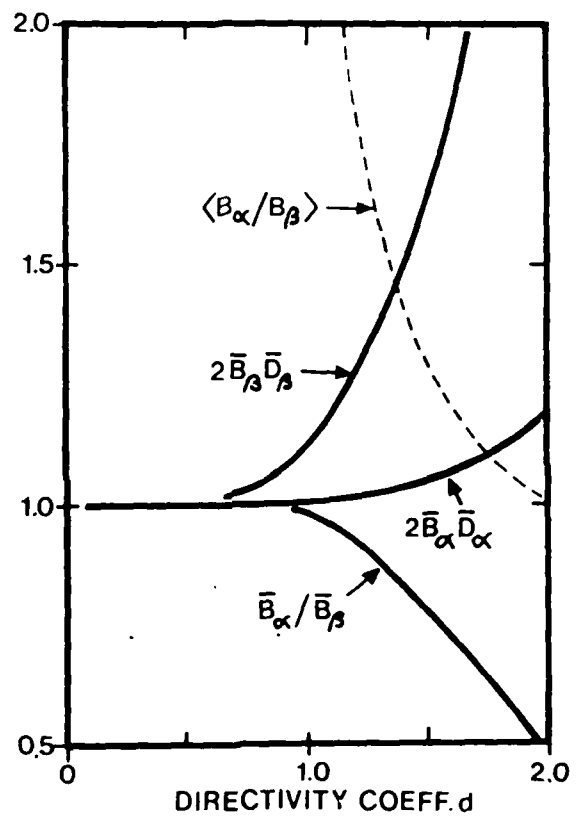


Fig. VI.2.1 Results for averaged spectral bandwidth and pulse width \bar{B}_c , \bar{D}_c , c the P or S velocity. A Gaussian spectral model has been used in the moment tensor approximation to the Haskell bi-directional model with aspect ratio 0.4. The directivity coefficient $d = \bar{F}_{xx}^2/(8\bar{F}_{tt}^2)$. For any point on the focal sphere $2\bar{B}_c\bar{D}_c = 1$, but the averaged values give in general $2\bar{B}_c\bar{D}_c > 1$. The dotted curve denoted $\langle B_\alpha/B_\beta \rangle$ gives the ratio of areas of the focal sphere where $B_\alpha > B_\beta$ and $B_\alpha < B_\beta$, respectively.

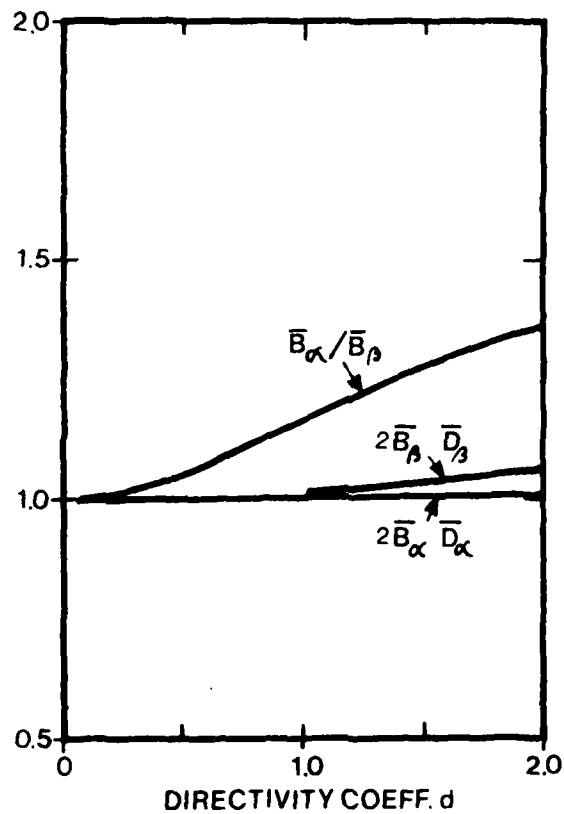


Fig. VI.2.2 Results for averaged spectral bandwidth and pulse width B_c , D_c , in a moment tensor approximation to a circular model. Other details as in Fig. VI.2.1.

VI.3 The new regional array: 1983 field experiments

The planning work for the new regional array to be installed in 1984 has continued during the reporting period. There have been extensive discussions between NORSAR personnel and representatives of the Sandia Laboratories, Albuquerque, New Mexico, which is the U.S. organization responsible for supplying and installing all hardware (seismometers, amplifiers, power cables, fiber optic cables for signal transmission, electronic equipment at the central site) for the new array. The new array will be deployed around NORSAR station 06C02 and according to status of the project as of November 1983 the new array should be operational by September 1984. This contribution gives a description of experiments with temporary field installations during the summer of 1983 and some preliminary results from analysis of the data collected. These experiments were undertaken in order to have a 'last minute' check on current design ideas for the 1984 array.

Borehole experiments

Results from a study of high-frequency noise recorded at the bottom of a 60 m deep borehole and comparison with simultaneously recorded noise at the surface have previously been reported by Bungum (1983). During 1983, PDR-2 recording equipment was operated in trigger mode to collect event data for the same experimental configuration. An example showing the P-phase from a local event at a distance of about 3° is given in Fig. VI.3.1. As is seen from the scaling factors the maximum amplitude of the signal is drastically reduced for the borehole record. Spectral differences are particularly pronounced above 8-10 Hz. It is suggested that the signal loss in the borehole is due to destructive interference of the direct P-wave with the surface reflected one. Crude calculations on wavelengths and time delays involved tend to support this assumption.

The problem at hand is that of finding the optimum depth of deployment of the 3-axis package to go into a borehole at the center of the new array. Data collected as described above in addition to borehole data collected in the U.S. will be evaluated to settle this question. An

uncertainty factor here is the coupling between the seismometers and the bedrock and its influence on recorded amplitudes at different frequencies.

3-axis experiment

During the period June 10-July 5, 1983, data were recorded on a 5-station array of 3-axis stations. The geometry of that array is shown in Fig. IV.1. During this period a number of local events were recorded.

The new array to be installed in 1984 will comprise 4 3-axis elements, whereof one will be located in a borehole at the center of the array. The location of the remaining 3 3-axis elements is still under consideration, and any one of the 24 remaining sites is and remains a possible candidate for deployment of 3-axis systems. The data collected this summer will now be subjected to analysis with the purpose of deciding where to deploy the 3 3-axis sets in the new array next summer.

21-channel array experiment

Theoretical work related to the design of the 25-element vertical array has been discussed by Mykkeltveit (1983). Discussions were held during the spring and early summer of 1983 between NORSAR personnel and representatives of Lawrence Livermore National Laboratory on the subject of the geometry of the new array. It was agreed to test the proposed geometry by a temporary installation during the summer of 1984. The temporary array became operational on July 25, 1983, and will be operated throughout the winter of 1984. It comprises 21 channels and its geometry is identical to that of the proposed 25-element array with the exception of 4 channels in the outer ring which have not been installed. The geometry of the temporary array is shown in Fig. IV.2. Analysis of the data recorded so far indicates that the geometry agreed upon is a very useful one, and the final decision has been made to implement it in 1984.

The correlation curves for signals and noise on which the proposed geometry was based have been confirmed by the new data as shown in Fig.

VI.3.2, providing a much denser sampling and broader range of intersensor spacings than available at earlier times.

The performance of the f-k analysis for detected phase arrivals will be of crucial importance to the on-line location capability of the new array. We are now in the process of collecting and analyzing data from events with known location (or location known to within a few km). Results of the f-k analysis (azimuth and phase velocity) for regional events analyzed so far are very promising. An example is given in Fig. VI.3.3 showing results from f-k analysis of the first P arrival (Pg) from a local event. F-k analysis is performed at 6 and 8 Hz, and the true azimuth to the event is 200°, which is also the azimuth resulting from the f-k analysis for both frequencies. For more results here, see Section VI.4.

S. Mykkeltveit
H. Bungum

References

Bungum, H., 1983: Seismic noise at high frequencies, NORSAR Semiannual Tech. Summ. 1 Oct 1982-31 Mar 1983.

Mykkeltveit, S., 1983: A new regional array in Norway: Design work, NORSAR Semiannual Tech. Summ., 1 Oct 1982-31 Mar 1983.

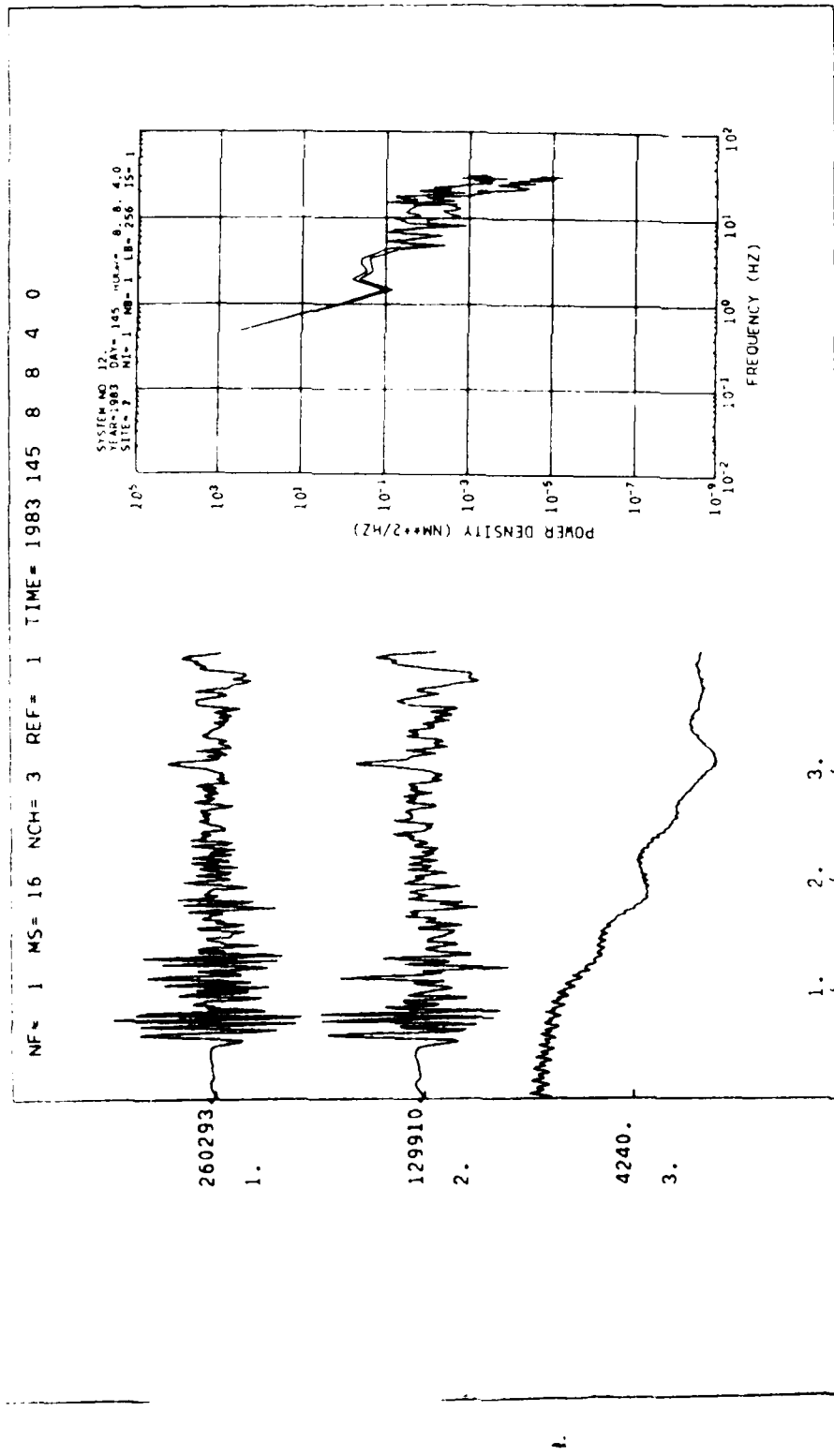


Fig. VI.3.1 P-wave signals and spectra for a local event at a distance of about 30'.
Channel 1: Surface recording. Channel 2: Recording at the bottom of a borehole.
Channel 3: Wind speed. Scaling factors to the left. Data sampling rate is 62.5 Hz.

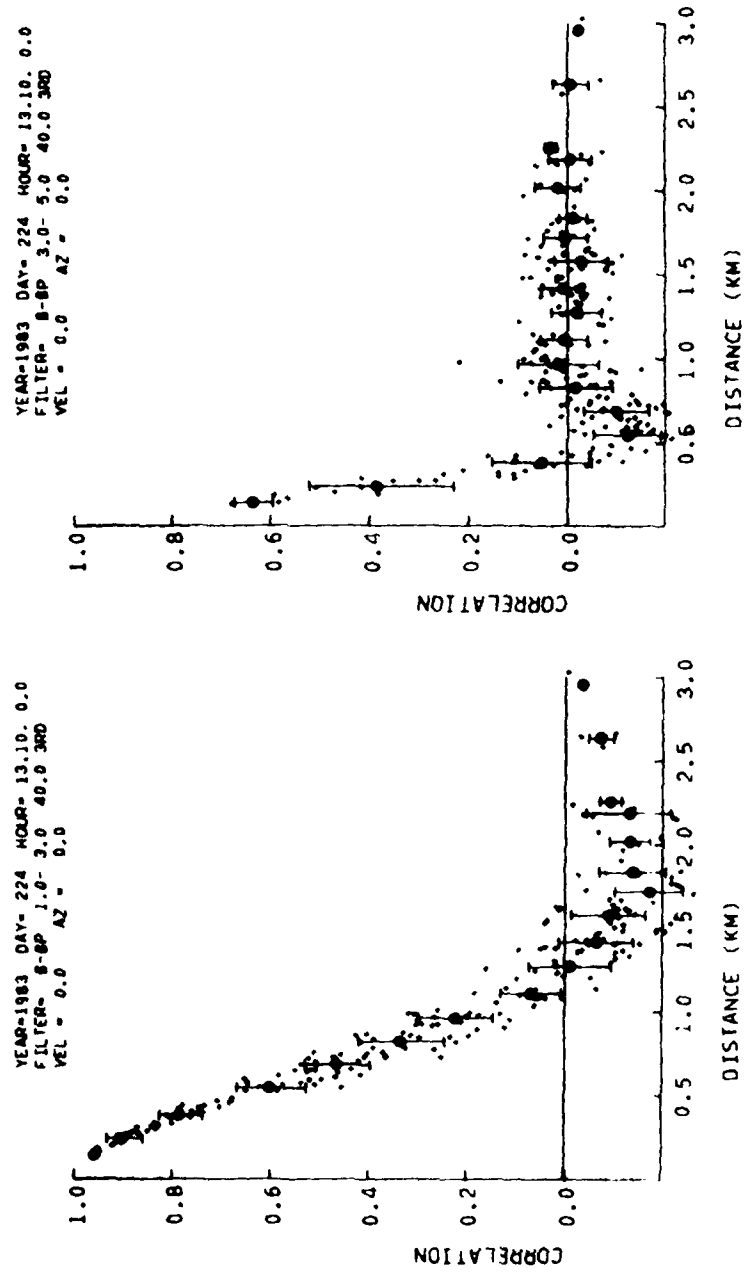


Fig. VI.3.2 Noise correlation curves for two frequency bands for the 21-element array. The data interval is 102.4 sec long. Mean values and standard deviations within separation intervals of 150 m are given by special symbols.

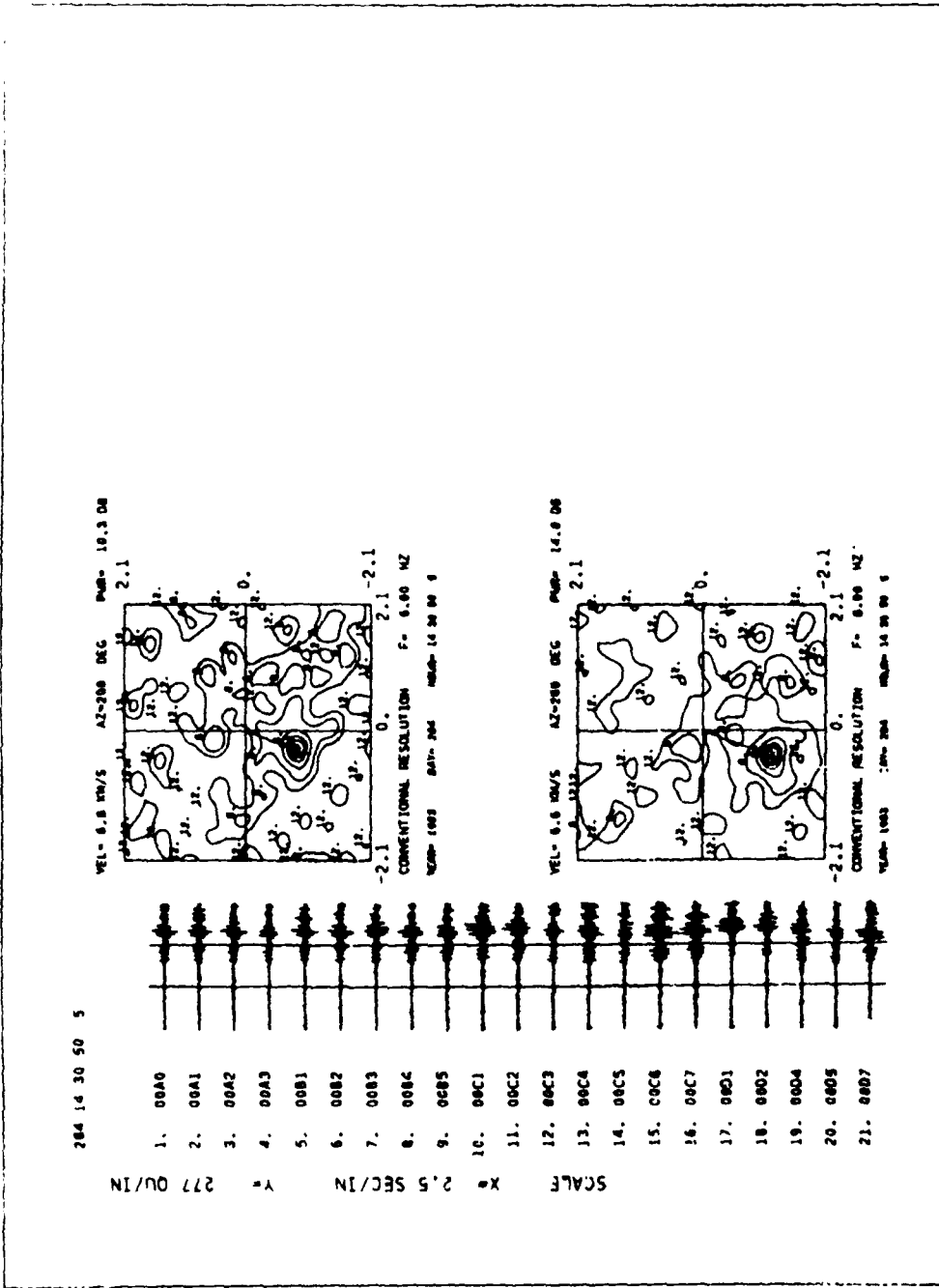


Fig. VI.3.3 Data from the new 21-channel vertical array for a local event at a true azimuth of 2000 and distance 118 km subjected to f-k analysis. The data window (between vertical bars) for f-k analysis contains the onset of the Pg phase. Data have been filtered 3-9 Hz before analysis.

VI.4 Further RONAPP developments

The RONAPP - Regional On-Line Array Processing Package - has now been developed further, and with two main changes:

1. To analyze the data from the new 21-channel test array in the NORESS siting area (see Section VI.3)
2. To include beam forming in the detector.

The first of these tasks was a trivial software job, but the second was not. To summarize what has been reported on previously (Mykkeltveit et al, 1982; Mykkeltveit and Bungum, 1983), the basic logic of RONAPP is as follows:

- 1) Initialize program, parameters, etc.
- 2) Event Detection Procedure: Enter a Detection Processor and stay there until a detection is found
- 3) Event Detection Analysis: When a detection is found, analyze the wave train causing the detection, essentially with the purpose of finding arrival azimuth and phase velocity
- 4) Event Location Procedure: If the wave train can be identified as an S (or Lg) phase, check with previous detections for a matching P phase, and perform an event location if possible
- 5) Return to 2) and continue.

Up to now, most of the RONAPP tests have been performed with data from a 6-channel test array, and an effort at that stage to include beam forming in the detector was not particularly successful because of beam space instabilities and associated problems with detection reductions. Because of this effect of a poor array configuration, most of the initial RONAPP analysis was based on detections from only one vertical beam.

The more recent changes in RONAPP can be described as follows:

- 1) The detection processor (DP) is initialized with any number of beams, each one specified in terms of azimuth, inverse velocity, filter, and individual channel weights. Time delays are then computed once and for all, and it will be easy at a later stage to include possible time delay corrections. The filter is normally the same for all beams

because of the beam space instabilities that otherwise would occur. The use of several filters would require equally many independent DP partitions, and this would only be a question of computer time.

- 2) The STA computations are now based on averaging absolute instead of squared amplitudes, in order to avoid precision problems in the computer and to save computer time. The corresponding loss in SNR is negligible.
- 3) For each beam, there is one STA/LTA threshold for declaring a detection (provided that P out of Q successive samples exceeds the threshold) and another (and lower) threshold for closing the detection.
- 4) The DP is defined to be in detection state if a detection is declared for at least one beam. To leave the detection state (i.e., to allow a new detection to occur), two criteria must be fulfilled:
 - All but a specified number of beams must be out of their (individual) detection state. (That number has so far mostly been set to zero.)
 - A certain time must have elapsed since the last beam closed its detection.
- 5) To process a detection (i.e., to enter Event Detection Analysis), a certain time must have elapsed since the previous processed detection.
- 6) Before a detection is processed, the beam with maximum STA is found and used as a basis for determination of refined arrival time, dominant frequency, f-k analysis prefilter, and f-k analysis time window.
- 7) Following each f-k analysis, the RONAPP procedure is unchanged, i.e., a phase association and event location procedure is entered if the last detection has been identified as an S-type phase. So far, our data base is too small for development of possible regional corrections in locations (systematic azimuth and phase velocity deviations), but with the present program structure the inclusion of such corrections should be quite straightforward software-wise.

This version of the RONAPP package has been tested on a number of selected events, as well as on real-time data. The performance with respect to an event (explosion) in western Norway is demonstrated in the following, with the seismic data shown in Fig. VI.4.1, and detections indicated by arrows.

We have previously had some problems with too many coda detections, a situation which now has been significantly improved with the availability of data from the new 21-channel array and with the new detection reduction procedures discussed above. The point with the coda detections is of course that they should be reduced in number without losing the detections that we are interested in.

The results for each detection are shown in the detection report on top of Table VI.4.1, and at the bottom of that table the results from phase association and location are given. It is seen there that the first location is based on the Sn phase combined with the Pn phase, a location which is recomputed upon the arrival of the stronger Lg phase. This is exactly the way we want the processing package to perform.

In Table VI.4.2 the results tied to one particular detection, namely, the Lg phase, are demonstrated. There are 13 beams (1 is vertical, 2-7 are P beams, 8-13 are Lg beams) which all have detected, but it is interesting to note that the best beam (no. 12) has an SNR of 140 while many of the others have around 30. This gives a ratio of about 4.7 which corresponds almost exactly to the beamforming gain that should be expected under ideal signal and noise conditions. It is seen further down in Table VI.4.2 that beam 12 is located (in slowness space) very close to where the f-k analysis finds maximum power.

H. Bungum
S. Mykkeltveit

References

Mykkeltveit, S. and H. Bungum, 1983: On-line event detection and location based on NORESS data. NORSAR Semiannual Tech. Summary 1 April - 30 September 1982.

Mykkeltveit, S., H. Bungum and F. Ringdal, 1982: A processing package for on-line analysis of data from small-aperture arrays. NORSAR Semiannual Tech. Summary 1 October 1981 - 31 March 1982.

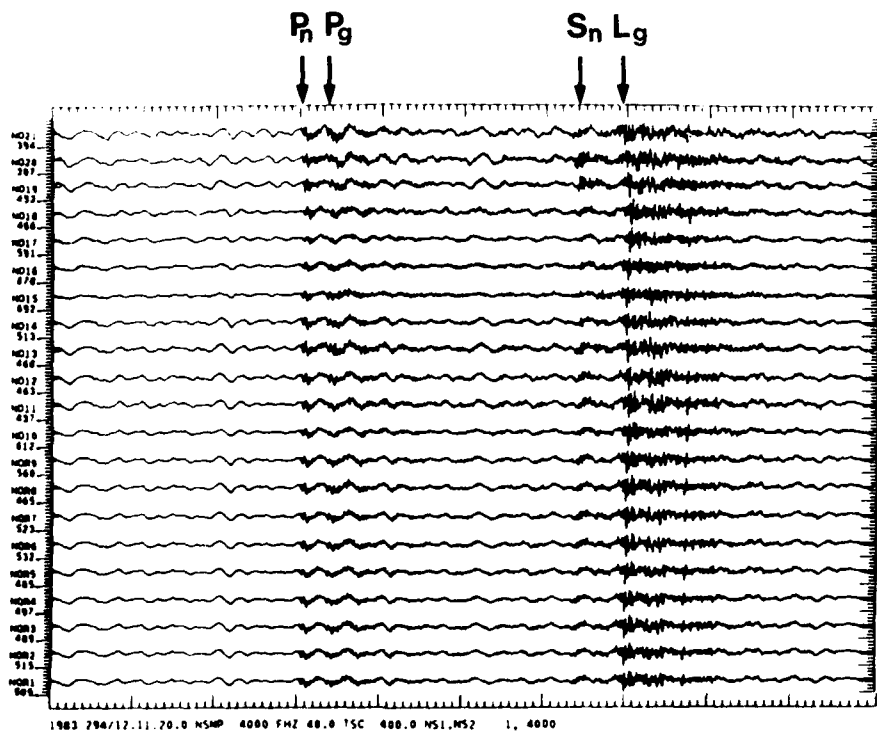


Fig. VI.4.1 Test event for RONAPP. The four phases indicated by arrows were detected, and only those. For each detection, the f-k results are displayed in Fig. VI.4.2.

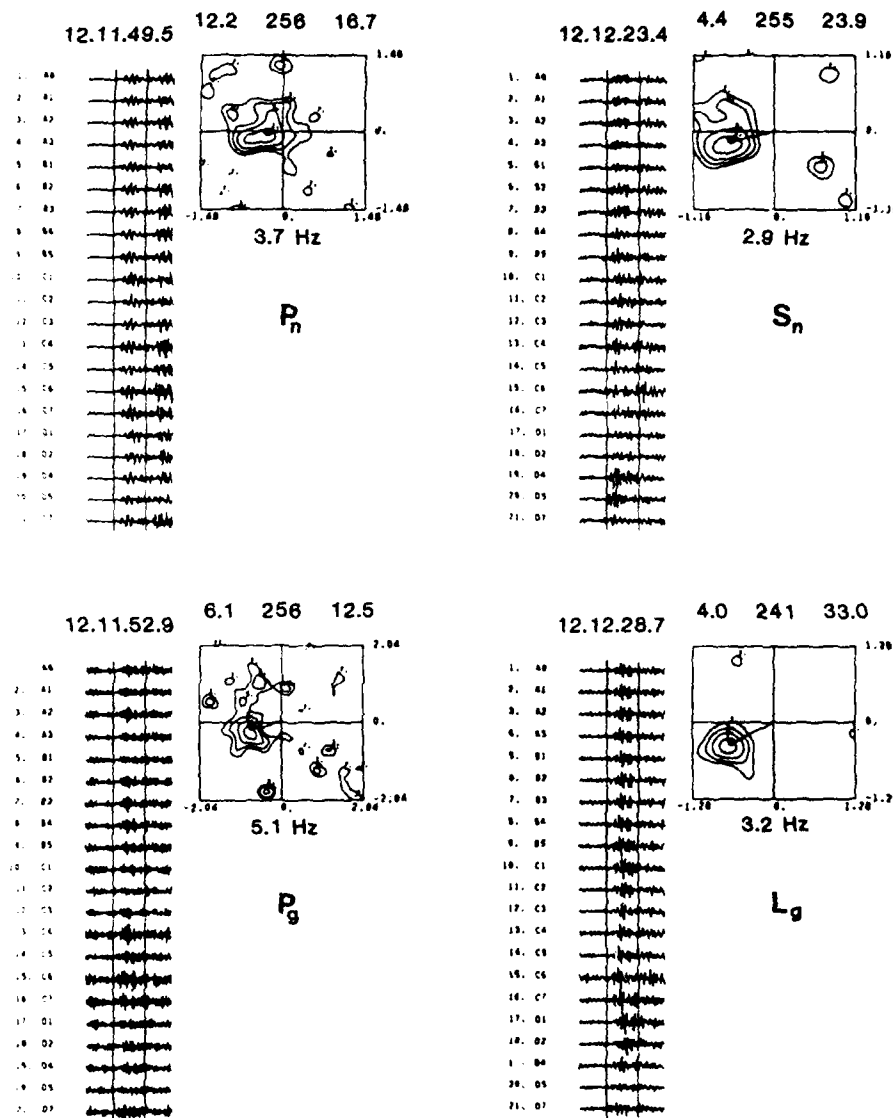


Fig. VI.4.2 Results from f-k analysis of the four detections in Fig. VI.4.1 (see also Table VI.4.1). The data used in processing are shown between bars (P_g is filtered 3-9 Hz, the others 2-8 Hz), and the numbers above the f-k plot indicate phase velocity (km/s), azimuth (degrees) and signal power (dB), respectively.

YEAR	DOY	TIME OF DAY	FN	AMPL	SNR	PER	FREQ	VEL	AZI	PWR	STA
1983	294	12 11 50	2	6 14	73.	4.13	0.27	3.70	12.13	256.0	16.6
1983	294	12 11 53	6	7 15	37.	4.37	0.20	5.10	6.06	256.0	12.5
1983	294	12 12 24	1	12 14	100.	4.17	0.34	2.90	4.39	254.7	23.9
1983	294	12 12 29	4	12 14	309.	4.19	0.31	3.20	3.99	241.4	32.9

LG TYPE PHASE DETECTED AT 1983 294 12 12 24 1
ASSOCIATED WITH P ARRIVAL AT 1983 294 12 11 50 2
EVENT LOCATED AT LAT, LON = 60.062 7.141

LG TYPE PHASE DETECTED AT 1983 294 12 12 29 4
ASSOCIATED WITH P ARRIVAL AT 1983 294 12 11 50 2
OVERRIDING EARLIER SOLUTION LAT, LON = 59.428 7.107 *

Table VI.4.1. Summarized detection listing from this run (top) and output from the phase association and location routine (bottom).

* RETURN TO DETECTOR *

BEAM	ICREL	ICABS	SNR
1	254	2814	31.7
2	256	2816	39.1
3	252	2812	30.4
4	275	2835	31.4
5	255	2815	38.6
6	253	2813	67.6
7	251	2811	56.4
8	252	2812	37.8
9	243	2803	31.8
10	273	2833	29.4
12	238	2798	140.6
13	255	2815	41.9

BEAM 12-1 DETECTED FIRST
BEAM 12-1 HAS LARGEST SNR (FIRST DETECTIONS ONLY)

DETECTION NO 1 : 294 12 12 29 9 (ICREL=238, ICABS= 2798)
REFINED ARR. TIME: 294 12 12 29 4 (ICREL=216)
HIRES START TIME : 294 12 12 28 7 (FREQ= 3.20)
BEAM NO 12-1 : AZI, VEL, STA = 240.0 4.5 140.6
HIRES RESULTS : AZI, VEL, PWR = 241.4 4.0 32.9

N	BM	ARR	REF	RMSN	STA	SNRT	AMP	PER	FREQ	VEL	AZI	PWR	AVDB
1	12	238	216	29.	141.	4.19	309.	0.31	3.20	3.99	241.4	32.9	13.0

* RETURN TO DETECTOR *

Table VI.4.2. Detector output for the last (Lg) detection in Figs. VI.4.1-2. Beam 12, with largest SNR, has an azimuth of 240° and a phase velocity of 4.5 km/s.

VI.5. Weighted beamforming in a real time environment

As is well known, the extent of signal and noise correlation between sensors in an array might significantly affect its performance in terms of suppressing the ambient noise while retaining signal integrity. The importance of signal and noise correlations as a function of sensor separations and frequency band has recently been demonstrated by Mykkeltveit et al (1983) in a scheme for optimizing array configurations. A rather obvious result here is that once the array becomes operational (configuration fixed) its performance is much dependent on dominant signal frequency. For example, a miniarrray designed for optimum detection capabilities for signals from local and regional events, say in the range 5-15 Hz, would be far less efficient for teleseismic signals in the frequency range 1-3 Hz. From a general seismological point of view, the preference is for array operation which is not strongly peaked as a function of frequency. In practice this requires that a flexible weighting scheme is introduced as part of the array on-line operation, where we try to capitalize on the information contained in the noise covariance matrix. The weighting technique used, to be briefly described in the following, is very similar to the optimum processing schemes developed by Capon, Lacoss and others (e.g., see Lacoss, 1974).

Signal/noise modelling and optimum weight estimation

Many weighting/filtering schemes have been developed for multichannel noise suppression. The best known class here is the Wiener filters which utilize the information contained in the autocovariance matrix, while in our scheme the subset hereof, the covariance matrix, is in focus.

Model I - Signals identical:

$$y_i = s + n_i ; \quad s = \text{signal, } n_i = \text{noise } i\text{-th sensor}$$

$$E(n_i n_j) = T_{ij}$$

$$\Sigma = (T_{ij}) = \text{noise covariance matrix}$$

Standard (unweighted) beams:

$$\hat{s} = \sum_{i=1}^k y_i = ks + \sum n_i$$

$$\hat{s} = k^2 s^2 + \ell' \sum \ell$$

$$\ell_{1,k} = \begin{Bmatrix} 1 \\ 1 \\ 1 \\ \vdots \\ \vdots \\ 1 \end{Bmatrix}$$

$$\text{Gain}^2 = \frac{k^2}{\ell' \sum \ell} = 10 \cdot \log \left(\frac{k^2}{\ell' \sum \ell} \right) \text{ dB}$$

Weighted beam:

$$\hat{s} = \sum_{i=1}^k w_i y_i = s \sum w_i + \sum w_i n_i$$

$$\text{Gain}^2 = \frac{(\ell' w)^2}{w' \sum w}$$

$$w_{ik} = \begin{Bmatrix} w_1 \\ \vdots \\ \vdots \\ w_k \end{Bmatrix}$$

By derivation of the gain function we find:

$$\max(\text{Gain}^2) \text{ for } w \sim \sum \ell$$

In practice we want to use a normalized weight function, and this introduces the w_{norm} -weights:

$$w_{\text{norm}} = \ell' w$$

$$w_{\text{use}} = w / w_{\text{norm}}$$

Implicit in this estimation scheme is that $\sum w_i = 1$. Important, in order to avoid negative weights, the w_i elements in the above gain

function are replaced by $w_i = x_i^2$. For $k < 20$ the minimizing of the gain function (is negative counterpart) can easily be performed directly without derivatives, etc.

Model II - Signals not perfectly correlated

In the case the gain would be:

$$\text{Gain}^2 = \frac{w' \Omega w}{w' \Sigma w}$$

with Ω being the signal covariance function.

Again, we can show that:

$$\max \text{Gain for } (\Omega - \lambda \Sigma) w = 0$$

where λ is the largest eigenvalue and w the corresponding eigenvector. We may also extend the model to include a priori knowledge of signal amplitudes (e.g., see Christoffersson and Husebye, 1974). Note that significant gain in beamforming is obtainable when sensor noise correlation is significant. Restricting weights to be positive only essentially amounts to 0/1 weighting.

Practical considerations

As in all other noise suppression schemes, the critical factor is noise stationarity, in this particular case the time/space stability of the noise covariance estimate in use. Parameters of importance here are:

- IW = length of data window for covariance estimate (2.5-10 sec); in average most stable results for IW = 10 sec or 400 samples
- INCR = covariance matrix updating rate; typical values 1.25-2.50 sec; in average most stable results for INCR = 2.5 sec or 100 samples
- ALFA = covariance matrix smoothing parameter; similar functioning of the STA/LTA sliding windows as used for signal detectors; here defined as ALFA = $1. - \text{EXP}(\text{ALOG}(1.-\text{PRO})/\text{FIW})$ with PRO = 0.5 and FIW = IW + 1

Now, parameters of importance in judging the performance of the above weighting scheme are as follows:

- TN = theoretical gain permitting negative weights tied to the covariance matrix only; no real data used
- ON = optimum gain (neg. weights permitted) as measured on the noise
- TP = theoretical gain for positive weights only
- PW = optimum gain for positive weights only
- ZW = only positive weights larger than 0.05 included
- SB = standard beam gain in signal-to-noise ratio (SNR).

The above gain measures are given in dB relative SB. It should be remembered that it is important to mask properly 'dead' traces, as these otherwise would be given very large weights in view of their vanishing variances. On the other hand, spikes would be efficiently removed as such traces have large variances.

Real-time simulation of weighting scheme

To test the performance of the above weighting scheme, a limited number of noise samples for the new, prototype NORESS array (see Fig. VI.5.1) have been used in data analysis. Due to disk storage restrictions, only 13 channels have been used at any type: i) sensor 1, B & C rings and ii) sensor 1, C & D rings. The inner A ring sensors have been consistently deleted due to small ranges, as their sensor separations are relatively small vis-à-vis the upper frequency 'cut-off' at about 4 Hz. These sensors may well be used, but presently strong transmission (electronic) noise prevails above this frequency, i.e., the provisional 60 dB dynamic range recording system does not permit adequate noise sampling over a wide frequency range. Typical noise data used in analysis is displayed in Fig. VI.5.2; filter setting 1.0-3.0 Hz 3rd order Butterworth. The strong correlation between sensors in the innermost rings is rather obvious.

Noise suppression capabilities

The optimum gain function (negative weights) is visually displayed in Fig. VI.5.2, while more detailed results are presented in Table

VI.5.1 for a typical noise sample. Not unexpectedly, the largest noise suppression is obtained for low frequencies, that is, where the noise is fairly well correlated. This is also shown in the rightmost column in the table, where the number of times a sensor has contributed constructively to the weighted beamforming is indicated. This is tied to the 'positive' weighting scheme, but the weights contributing by less than 5% are zeroed while the remaining are set equal to 1. The total number of updating intervals was 44, so some sensors are truly abundant. The corresponding relative gain is listed in the ZW-column.

Some interesting features of Table VI.5.1 are as follows:

- the noise suppression is azimuth-dependent
- the weighting gain appears to be velocity-dependent, relatively best performances for surface wave phase velocities (4.6 km s^{-1}) and teleseismic P-velocities (12 km s^{-1})
- the weighting scheme can produce gains in excess of \sqrt{N} .

A similar experiment was performed by replacing the B-ring sensors with those of the D-ring (see Table VI.5.2). The outstanding feature here is the gain from weighted beamforming is very small, occasionally even negative. The reason for this is non-stationarity in the noise field when sensor separations become relatively large. The theoretical gain in this case is not too different from that of the previous and furthermore well above 1 dB. The latter data are not shown here.

The noise suppression is from Tables VI.5.1 & VI.5.2 obviously azimuth-dependent, and this feature has been further investigated. In Table VI.5.3 gain as a function of small azimuth intervals is displayed. Interestingly, for those azimuths where the gain (SB) is the smallest, the most contributing sensors (underlined in the rightmost column) form triangles (squares) whose longest axis are roughly perpendicular to the azimuth in question (the OK notation in the AC column). This we interpret in terms of stronger correlation in the noise in the direction of propagation (radial) than in the transverse direction, which is indeed expected for scattering

phenomena (Chernov, 1960). In other words, the correlation in the noise appears to depend on both sensor separation and their relative orientation. The latter feature, if prominent, would clearly have a bearing on the array configuration optimization schemes. For example, the approach of Mykkeltveit et al (1983) essentially amounts to a noise covariance matrix model with zeros or small negative values for all off-diagonal elements. We have not observed this during our analysis so far nor obtained a gain exceeding \sqrt{N} for standard beamforming (SB). This is a bit puzzling as noise correlations as a function of sensor separations only have been observed to exhibit a small negative minimum of the order of 0.1 units. This discrepancy may reflect a certain non-stationarity in the noise field in short intervals as used here, although the above-mentioned noise covariance matrix model is likely to represent an oversimplification of the real noise field. Thus, if the off-diagonal elements cannot be ensured to be zero or negative, the consequence of this is that the center station seldom would contribute constructively towards noise suppression by beamforming. This is quite obvious from the results presented in Tables VI.5.1-3 for the lower frequency bands.

Discussion and conclusion

A preliminary evaluation of the provisional regional array installed within the NORSAR array has been made. It is somewhat incomplete in the sense that the operational settings of the array up to now only permit analysis in the frequency band 1 to 4 Hz and thus excludes the most important frequency band for small local and regional events, say 1.5 to 3.5 m_b units, namely, 5 to 15 Hz. Anyway, the main results obtained are as follows:

- When there is a significant tie in the noise data, weighted beamforming would produce an additional noise suppression gain of the order of 1 to 3 dB, roughly equivalent to 10-30% operational improvement.
- The noise field must be rated non-stationary as significant changes in the noise covariance take place within 5 to 10 sec interval. In this respect claimed long term noise stationarity features

like negative correlation values in certain sensor separation ranges appear to be very modest, at least in comparison to relatively strong short term variations.

- A certain directability in the noise field is apparent for certain azimuth directions. In practice this gives reduced noise suppression capabilities or an equivalent higher false alarm rate on certain beams.
- Array configuration optimization; this is a problem if reasonable performance is desired over a relatively wide frequency range. Optimum processing schemes appear to be unavoidable here or the array must compromise on a duality in configuration.
- Finally, optimum weighting schemes are rather time-consuming in practice and can hardly be 'afforded' unless there is access to an array processor for handling the covariance matrix 'inversion' task. We are pursuing this problem now, the motivation being that this would be very cost effective per unit dB gained in noise suppression of small arrays.

E.S. Husebye
S.F. Ingate
A. Christoffersson, Univ. of
Uppsala

References

Chernov, L.A., 1960: Wave Propagation in a Random Medium, McGraw-Hill Book Co., New York.

Christoffersson, A. & E.S. Husebye, 1974: Least squares estimation techniques in analysis of seismic array recorded P-waves, Geophys. J. R. Astr. Soc., 38, 525-552.

Lacoss, R.T., 1974: Review of some techniques for array processing.
in: K.G. Beauchamp (ed.) Exploitation of Seismograph Networks,
Nordhoff Intern. Publ., Leiden, the Netherlands, pp. 11-23.

Mykkeltveit, S., K. Åstebøl, D.J. Doornbos & E.S. Husebye, 1983: Seismic array configuration optimization, Bull. Seism. Soc. Am., 73, 173-186.

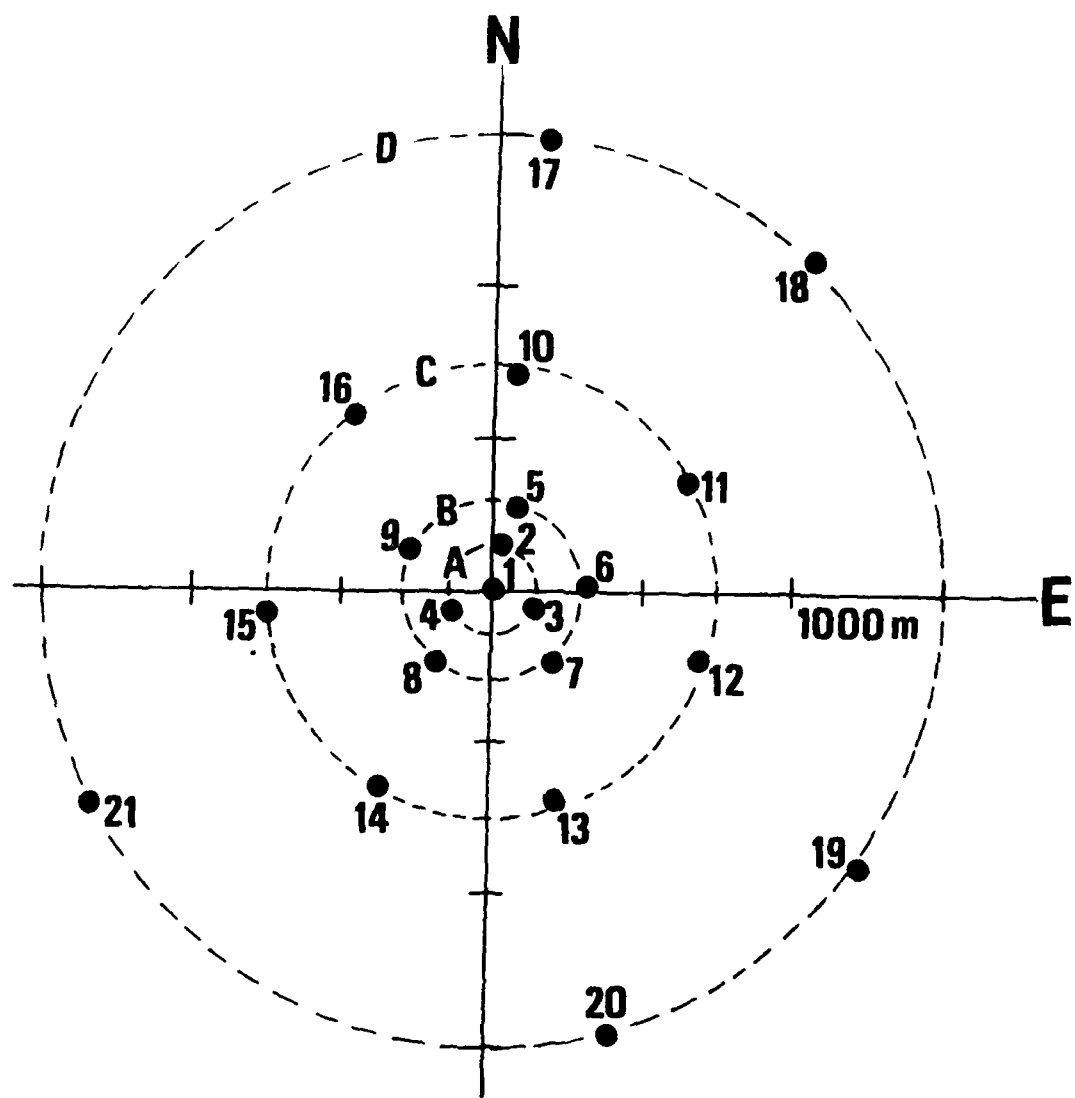


Fig. VI.5.1 The prototype NORESS array, data from which are used in this analysis.

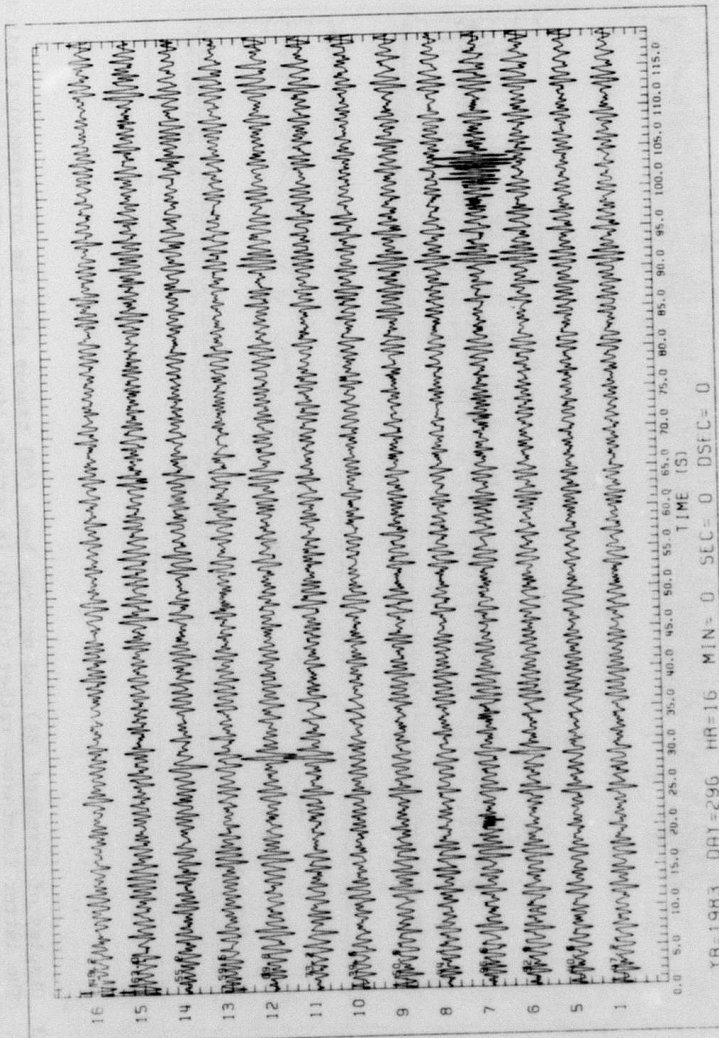


Fig. VI.5.2 Noise data used in analysis. Sensor numbering and rms-scaling on the vertical axis while the horizontal axis gives the time intervals (sampling rate 40 Hz). Filter 2 was used, i.e., the 1.0-3.0 Hz pass band.

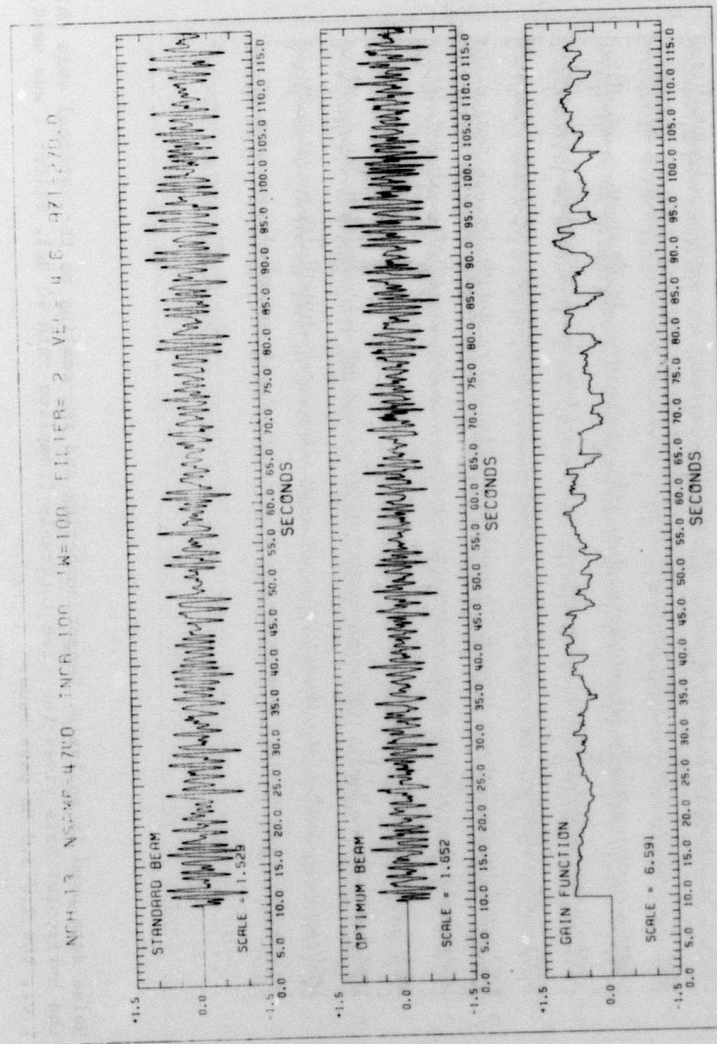


Fig. VI.5.3 Display of standard (BS) and optimum beam (ON) traces plus the corresponding gain function. The latter fluctuates rather rapidly in certain time intervals which we take to reflect a certain non-stationarity in the ambient noise.

Filter	Vel.	Az.	Gain	Al				B-ring				C-ring							
				SB	NW	PW	ZW	1	5	6	7	8	9	10	11	12	13	14	15
2	4.6	0	3.63	2.41	1.19	1.14	0	8	0	1	3	0	30	37	32	44	18	44	35
2	"	90	2.46	2.51	1.10	1.07	0	1	0	0	0	0	41	16	5	42	39	15	42
2	"	180	3.94	2.15	1.47	1.45	1	6	0	2	0	0	27	40	24	40	21	44	44
2	"	270	5.24	2.73	1.91	1.84	0	10	0	0	4	0	41	28	31	32	43	44	41
3	6.2	0	6.50	0.81	1.00	0.95	5	21	2	0	3	1	38	44	42	40	42	44	40
3	"	90	5.34	1.12	1.27	1.18	4	7	2	4	2	0	41	37	28	44	44	22	43
3	"	180	5.25	0.80	0.79	0.69	12	12	0	1	20	1	26	31	41	33	29	38	43
3	"	270	6.71	1.14	1.17	1.08	2	28	2	0	17	2	36	35	33	43	36	40	42
4	8.1	0	10.0	1.29	1.37	1.06	20	40	13	1	33	11	36	42	42	43	40	41	43
4	"	90	8.82	1.26	1.41	1.12	24	17	1	6	19	9	44	30	44	44	42	42	44
4	"	180	7.81	0.95	1.13	0.92	20	23	3	6	22	8	42	33	44	42	39	24	44
4	"	270	9.79	1.12	1.18	0.78	9	30	21	1	41	24	41	38	42	44	36	32	44
5	12.0	0	11.29	2.64	2.61	2.09	24	40	38	0	38	31	42	36	44	44	38	28	44
5	"	90	10.42	1.87	1.96	1.49	25	26	10	1	25	18	43	37	44	44	37	27	44
5	"	180	9.94	1.86	2.00	1.61	27	22	10	3	31	12	44	24	44	44	42	29	44
5	"	270	11.14	2.21	2.22	1.73	27	26	34	0	41	33	42	41	44	44	32	23	44

Table VI.5.1 Various measures of beamforming gains as a function of filter setting, velocity and azimuth. The Butterworth filters used are respectively 2: 1.0-3.0 Hz; 3: 1.5-3.5 Hz; 4: 2.0-4.0 Hz; and 5: 2.5-4.5 Hz. SB = gain (in dB) on the standard (unweighted) beam. The NW, PW and ZW columns give gain (in dB) relative to SB for beamforming based on both positive and negative weights, positive weights only and positive weights larger than 0.05, respectively. The columns associated with the Al, B- and C-ring sensors (see Fig. VI.5.1) indicate the number of times a sensor contributed to the ZW-beamforming scheme. For example, for filter 2 most of the Al & B-ring sensors hardly contribute to the noise suppression; their weights are less than 0.05, and besides the difference between PW and ZW gains is quite small. Total number of trials was 44.

Filter	Vel.	Az.	Gain			A1			C-ring			B-ring							
			SB	NW	PW	ZW	1	10	11	12	13	14	15	16	17	18	19	20	21
2	4.6	0	6.88	0.25	0.38	0.19	10	0	21	18	24	27	36	24	41	15	44	42	44
2	"	90	5.20	1.15	1.35	1.30	21	7	2	17	10	11	19	22	44	44	17	44	11
3	"	0	9.38	-0.36	-0.31	-0.88	9	13	17	29	17	30	29	30	44	44	42	40	44
3	"	90	8.26	0.48	0.57	0.26	8	35	34	15	36	22	3	26	44	38	26	44	43
4	"	0	10.73	-0.21	-0.21	-0.90	41	34	31	39	17	28	8	34	43	40	31	34	44
4	"	90	10.10	0.22	0.25	-0.13	39	44	31	13	44	34	0	40	44	30	19	42	44
5	"	0	10.58	0.18	0.19	-0.36	44	31	40	44	21	40	0	36	44	23	16	35	44
5	"	90	10.39	0.09	0.13	-0.33	44	44	43	36	44	32	0	43	44	6	10	40	29

Table VI.5.2 Caption similar to that of Table VI.5.1. Notice that a larger array configuration is used this time

Filter	Vel.	Az.	Gain			A1			B-ring			C-ring							
			SB	NW	TG	AC	1	5	6	7	8	9	10	11	12	13	14		
2	4.6	0	3.63	2.73	3.54	-	0	5	0	0	1	0	32	41	35	44	19	44	39
"	"	30	2.92	2.00	3.34	ok	0	0	0	0	0	0	36	17	29	44	7	44	42
"	"	60	2.47	2.69	3.30	ok	0	0	0	0	0	0	39	21	8	44	21	33	44
"	"	90	2.46	2.77	3.50	ok	0	0	0	0	0	0	44	15	3	44	43	13	44
"	"	120	2.80	2.52	3.44	ok	0	0	0	0	0	0	44	25	3	40	44	36	18
"	"	150	3.28	2.33	3.36	-	0	0	0	0	0	0	44	36	15	29	42	42	15
"	"	180	3.94	2.29	3.45	ok	1	23	0	0	0	0	40	43	23	34	26	44	30
"	"	210	4.54	3.12	3.97	-	0	4	0	0	0	0	30	42	27	42	21	44	44
"	"	240	4.96	3.27	4.12	-	0	2	0	0	0	0	42	41	31	44	33	44	44
"	"	270	5.24	3.05	3.90	-	0	5	0	0	2	0	42	34	38	41	44	44	42
"	"	300	4.92	3.03	3.92	-	0	7	0	0	0	0	43	43	41	19	44	44	21
"	"	330	4.35	2.97	3.86	-	0	0	0	2	0	0	41	44	39	25	43	44	22

Table VI.5.3 Caption similar to that of Table VI.5.1. TG = theoretical gain (both negative and positive weights) while the array configuration (AC) column indicates for which azimuth direction there seems to be noise orthogonality, i.e., the noise correlation is more prominent in the radial (azimuth) than in the transverse direction. The most contributing sensors (underlined) form triangles or squares whose principal directions are roughly perpendicular to the beam azimuth.